Statistical analysis of off-lattice diffusion-limited aggregates in channel and sector geometries

A. Arneodo, J. Elezgaray, M. Tabard, and F. Tallet
Centre de Recherche Paul Pascal, Avenue Schweitzer, 33600 Pessac, France
(Received 16 October 1995)

The statistical properties of off-lattice diffusion-limited aggregates (DLA) grown in a strip between two reflecting walls are investigated. A large number of independent runs are performed and the cell occupancy distribution is measured and compared with the predictions of a recently proposed mean-field theory (MFT). It is shown that the mean occupancy profile moves at constant speed and has a shape and a selection mechanism similar to that of stable Saffman-Taylor fingers. In particular, there exists a specific contour line of the mean occupancy distribution ($\rho=0.6\rho_{\max}$) that has the width and the shape of the Saffman-Taylor finger $\lambda=0.5$. Motivated by the connection to the Saffman-Taylor problem, we extend our study to DLA growth in sector-shaped cells. Again a remarkable agreement is found between the mean occupancy profile and the shape of the selected stable finger in the small surface tension limit. Moreover, whenever the smooth finger is theoretically expected to undergo a tip-splitting instability, one observes, as predicted by the MFT, a qualitative change in the cell occupancy distribution that exhibits ''profile crossing'' together with a pronounced flattening of the tip region. We comment on this phenomenon, which was not observed in a previous similar statistical analysis of on-lattice DLA clusters due to the stabilizing effect of lattice anisotropy. The implications of our numerical results to the relevance of the DLA mean-field theory are discussed. [S1063-651X(96)06905-8]

PACS number(s): 68.70.+w, 61.43.Hx, 47.15.Hg, 47.20.Hw

I. INTRODUCTION

In recent years, diffusion-controlled growth phenomena have attracted a lot of interest [1–15]. Notable examples [16–18] of interfacial pattern formation in diffusive systems range from viscous fingering to electrochemical deposition and to the growth of bacteria colonies. Among this wide variety of systems, the Saffman-Taylor (ST) fingering [19] in two-dimensional Hele-Shaw cells is without any doubt the one that has received the most attention [3–6,20]. Experimental and theoretical efforts have been mainly focused in two directions. On the one hand, the shape and selection mechanisms of nonlinear stable smooth curved fronts were investigated and analytical solutions were found in various geometries [3–6,19–21]. On the other hand, the very unstable branched patterns observed when either decreasing surface tension or increasing the width of the cell have been mainly considered from the point of view of their fractal structure [21–29].

The instability giving rise to ST viscous fingering [19,30] occurs at the interface between two fluids moving between narrowly spaced solid plates. The interface is unstable when the less viscous fluid forces the most viscous fluid to recede. The flow of the fluid is dominated by the viscous dissipation on the plates and the mean velocity in the cell plane is proportional to the pressure gradient $\vec{V}=-(b^2/12\mu)\nabla p$, where b is the cell thickness and μ the viscosity of the most viscous fluid. Because of the incompressibility of the fluids, the pressure field obeys a Laplace law $\Delta p=0$. Surface tension has a stabilizing influence [3]; this is taken into account by adding a boundary condition for the pressure jump at the interface: $[p]=T\kappa$, where T is the surface tension and κ the local curvature of the meniscus in the plane of the cell. The linear stability analysis [30] of a plane interface moving at constant velocity $\vec{V}$ gives the wavelength of maximum instability: $l_c=\pi b(T/\mu V)^{1/2}$. The capillary length l_c can be seen as the characteristic small length scale of viscous fingering.

In the configuration originally chosen by Saffman and Taylor [19], the fluids move in a very long linear channel of width W. In this geometry, the boundaries somewhat simplify the problem by imposing translational invariance. The control parameter is usually defined as the following dimensionless number [3,21]: $B=(1/12\pi^2)(l_c/W)^2$, which is proportional to the square of the ratio of the smallest (l_c) to the largest (W) characteristic length scales of the system. Whenever these two length scales are close to each other ($l_c/W>1/8$, $B>1/768\pi^2$), the injected less viscous fluid takes the shape of a single finger that moves through the cell at constant velocity [21]. In their pioneering work, Saffman and Taylor [19] showed that the shape of the finger can be obtained from effective two-dimensional (2D) equations when the surface tension between the two fluids is neglected ($T=0$). In this approximation, the shape is not entirely determined but rather a one-parameter family of shapes exists, the free parameter being the ratio λ ($0\leqslant\lambda\leqslant1$) of the width of the finger to the width of the channel:

$$x(y)=\frac{W(1-\lambda)}{2\pi}\ln\left[\frac{1}{2}\left(1+\cos\frac{2\pi y}{\lambda W}\right)\right] \qquad (1)$$

($0x$ corresponds to the direction of propagation of the finger). The experiments [21,31] show, however, that the finger tends to occupy half of the channel at small values of the parameter B (e.g., at large velocities). The selection of the observed asymptotic finger width $\lambda=0.5$ was understood rather recently after numerical investigations [32,33] and analytical works [34–36]. Acting as a singular perturbation, surface tension selects, out of the continuum Saffman-Taylor family [Eq. (1)], a discrete family of finger shapes [$\lambda_n(B)$] that all merge when T (i.e., B) tends to zero. Among this family, only the branch defined by the narrowest of these

shapes ($\lambda_{n=0}$) corresponds to linearly stable fingers. Actually, when the parameter B becomes too small, the two characteristic length scales $l_{\min}=l_c$ and $l_{\max}=W$ depart significantly from each other and one observes experimentally the destabilization of the smooth finger into an arborescent structure with a fractal-like appearance [21,27,29]. As pointed out in Refs. [5,6,19], this phenomenon can be understood as a noise-induced jump from the stable to the unstable branches of finger shapes that is possible only for small values of B, when different branches are getting very close to each other.

Since in Laplacian pattern forming systems, the motion of the interface depends upon the boundary conditions fixed by the cell shape, the choice of the geometry is crucial [21]. As a very clever generalization of the Hele-Shaw geometry [41], Thomé *et al.* [42] have proposed to study viscous fingering in a wedge of arbitrary angle θ_0; this sector geometry provides a natural bridge between the linear [19,41] and the open circular [43,44] geometries. It was observed that, as in Hele-Shaw cells, for large enough velocity, a unique finger tends to occupy a well-defined angle fraction of the sector cell. The difficulty of experiments in a wedge comes from the unsteadiness of the growth [42]. If the front velocity is kept constant, thereby fixing the capillary length l_c, then the dimensionless parameter B varies during the growth since the local width $W(r)=r\theta_0$ of the cell is a function of the distance r of the front to the apex ($B\sim 1/r^2$). B increases in convergent cells ($\theta_0<0$) and decreases in divergent ones ($\theta_0>0$). Only if B is maintained artificially constant by adjusting the velocity so that it varies as $V\sim 1/r^2$ will the finger have a self-similar growing shape. For a given value of B, its angular width scales on the cell angle θ_0. For all convergent cells, the relative angular finger width $\lambda(\theta_0,B)$ is observed to converge towards an asymptotic value $\lambda(\theta_0)<\frac{1}{2}$ in the limit B tends to zero. Moreover, this fraction $\lambda(\theta_0)$ is an increasing function that approaches $\frac{1}{2}$ as θ_0 approaches $\theta_0=0$, i.e., the value corresponding to linear cells. For divergent cells, similar single smooth fingers of relative width $\lambda(\theta_0)>\frac{1}{2}$ are formed whenever B takes on values above some critical threshold $B_c(\theta_0)$ that turns out to be an increasing function of θ_0 [42]. Whatever the value θ_0 of the cell angle, below this critical parameter value $B<B_c(\theta_0)$, smooth self-similar fingers are unstable. Very much like what has been observed in linear cells, when the ratio W/l_c is large, the range of scales available to fractal branching is large enough for treelike structures to develop [21,42].

From a theoretical point of view, a lot of effort has been devoted recently to generalizing the shape, selection, and stability analysis of steady-state fingers in linear cells to smooth fingers growing in sector-shaped cells [20,45–49]. This amounts to a switch from a growth problem in a geometry that is translational invariant to a geometry that is invariant under rescaling. In the limit of zero surface tension, for each value of the sector angle θ_0, a one-parameter family of self-similar finger solutions parametrized by their relative angular width $\lambda(\theta_0)$ was analytically found [46] as the counterpart of the Saffman-Taylor solution family in a linear channel. The role of surface tension in finger selection has been investigated numerically and analytically with very interesting results [46–49]. For convergent sectors of arbitrary angle $\theta_0<0$, a discrete family of solution branches $[\lambda_n(\theta_0,B)]$ is selected; they all converge to a self-similar finger profile of finite angular width $\lambda(\theta_0)$ in the limit B goes to 0. As in linear geometry, the branch defined by the narrowest fingers corresponds to the observed stable solutions. A surprising result was, however, obtained for divergent sectors. A discrete family of branch solutions always exists for any sector angle θ_0 at rather large B values. But these branches $[\lambda_n(\theta_0,B)]$ no longer approach a unique limiting shape as B tends to zero since different branches merge by pairs and successively disappear before the limit of zero surface tension is reached. As emphasized in Ref. [46], the merging of the first two lower branches [the lowest one $\lambda_{n=0}(\theta_0,B)$ corresponding to the stable fingers] is likely to correspond to a tip-splitting instability for the smooth finger [20,21]. Therefore, on the contrary to the situation encountered in linear or convergent sector-shaped cells, the destabilization of the finger into an arborescent fractal structure in divergent cells turns out to be intrinsic and noise independent. Moreover, since most of the experiments are performed at constant applied pressure [42], there is no way to escape from this instability; actually the finger velocity slows down like $1/r$, which implies that $B(\sim 1/r)$ decreases irreversibly during the growth process. Thus, in these experiments, one follows dynamically the branch of stable solutions, ultimately reaching the critical point $[B_c(\theta_0)]$ where this branch disappears. The theoretical band-merging scenario [46–49] therefore provides a comprehensive understanding of the experimental observation that in a divergent sector, whatever the angle θ_0, a single smooth finger is always observed as a transient towards a more complicated morphological evolution. As the result of a competition between tip-splitting instabilities and screening effects, the system evolves asymptotically towards some apparently disordered arborescent pattern that is likely to display scale-invariance properties [21,42].

Among the various models of stochastic growth proposed for fractal aggregates [12], the diffusion-limited aggregation (DLA) model introduced by Witten and Sander [50] is well known to produce self-similar ramified patterns that strongly resemble the unstable viscous finger morphologies observed in the unsteady regime [21–29]. In this model, random walkers are sent, one at a time, from far away and the structure grows via irreversible sticking when the walker reaches a neighboring site of the preexisting aggregate. As was first noted by Paterson [22], the equations of growth of DLA are similar to those of ST fingering in the limit of zero surface tension. In the numerical model of random walking particles, the role of pressure is played by the probability P to visit of a site; P similarly obeys a Laplace law $\Delta P=0$ and the normal velocity of growth of a region of the interface is $V_n \propto(\nabla P)_n$. The difference between the two descriptions comes, of course, from their deterministic or stochastic nature but also from the existence of surface tension in viscous fingering, which has no obvious counterpart in DLA. Let us note, however, that the computation of DLA clustering is usually performed on a lattice and that the lattice mesh size l_u introduces a smallest length scale $l_{\min}$ in the simulation [21,29]. But that does not mean, *a priori*, that the probability P satisfies the boundary condition $[P]=T\kappa$ at the interface.

Several experiments and numerical simulations were devoted to the comparison of the fractal branched patterns obtained in viscous fingering and DLA clusters [3,12,21–

28,51–56]. More remarkable is the connection recently found in Ref. [57], between the ramified DLA structures and the smooth stable viscous fingers. The computation of the ensemble-averaged DLA pattern, which of course is a rather smooth and orderly structure, has revealed a mean profile that coincides with the (finger) shape of the smooth analytical solution. Furthermore, the selection of a particular finger width, generally ascribed for stable fingers to the effect of surface tension, apparently survives the instability and still governs, at least in a statistical sense, the growth in the fractal regime. For example, in a linear channel, the average DLA structure defined by the points of the cell whose occupancy probability is above average, is almost exactly the $\lambda = \frac{1}{2}$ Saffman-Taylor finger. This statistical analysis has been extended to sector geometries [57], to the case of anisotropic growths [58,59], and to the unstable side branchings of fractal dendrites [58]. These studies all confirm the unexpected feature that Laplacian growth processes seem to retain, in the unstable fractal branching regime, some memory of the shape and selection mechanism of the stable finger structure [29].

In order to explain the above correspondance, a mean-field theory (MFT) has been proposed recently for two-dimensional DLA, both in linear [60] and sector [61] geometries. This theoretical approach is directly inspired by the mean-field equations established by Witten and Sander [50] in their pioneering work that couple a walker field to an aggregate field. The main modification is the introduction of an additional parameter that is supposed to account for the intrinsic discreteness of the sticking process in the DLA model. The comparison between the MFT predictions and the occupancy probability distributions computed in DLA simulations yields satisfactory results as long as the ensemble average is performed on small-size (or small-mass) DLA clusters. This remarkable agreement provides some understanding of the relationship discovered experimentally between ramified DLA structures and smooth selected finger patterns [57]. Some severe discrepancies seem nevertheless to arise when one proceeds to large-mass DLA simulations, e.g., in very wide linear cells or in divergent sector cells when one does not stop the simulation early enough before entering some crossover regime towards dendritic growth [58,59]. Large-mass DLA clusters grown on a square lattice are known to display preferential directions of growth [62–71]. One can easily imagine that the anisotropy inherent to on-lattice DLA simulations may completely alter its ensemble-averaged behavior at macroscopic scale. In Ref. [61], Levine and Tu have demonstrated that adding phenomenologically anisotropy in the MFT modifies the overall shape of the aggregate field in such a way that it correctly describes the average DLA structures. Here, our aim is to take the opposite task and to get rid of the underlying lattice anisotropy by performing DLA simulations with an off-lattice algorithm [72–75]. Then we will be in position to proceed to a direct comparative test of the relevance of the MFT, keeping in mind, as a reference shape, the corresponding ST finger solution when it is stable.

The paper is organized as follows. Section II is devoted to the comparison of averaged off-lattice DLA patterns and MFT predictions in linear channels. This study is extended to sector-shaped cells in Sec. III. Our conclusions are summarized in Sec. IV.

II. LINEAR GEOMETRY

A. Off-lattice DLA simulations

To generate isotropic DLA clusters in a strip with reflecting walls, we have adapted a very efficient off-lattice algorithm originally designed by Tolman and Meakin [72], and previously used for simulating DLA growth in circular geometry [73–75]. This algorithm combines the simplicity of the off-lattice algorithm proposed in Ref. [76] with the rapidity of the on-lattice hierarchical algorithm [62] (we use the following conventions: we choose $0x$ along the cell axis and $0y$ across the cell). Initially, a circular particle of diameter a is launched at a random position on a line parallel to the linear substrate and located at a distance $x_{\max}+l$ from it, $x_{\max}$ being the abscissa of the particle of the cluster the furthest from the basis and l is a few times the particle diameter (practically $l=3a$). Then, at every step, the distance $d_{\min}$ of the walking particle to the closest point of the cluster is determined: if $d_{\min}<a$, the diffusing particle stops and becomes part of the cluster by sticking to the closest cluster particle previously determined. Otherwise it jumps to a random position on a circle of radius $R=d_{\min}-(1-\delta)a$, where $0\leqslant\delta\leqslant 1$ is an overlapping parameter. According to standard practice, the diffusing particle is lost if its distance to the linear substrate exceeds some critical value $x_c=4x_{\max}$. As far as the efficiency of the algorithm is concerned, the calculation at each step of the distance $d_{\min}$ of the diffusive particle to the aggregate can be very time consuming. To make practical the computation of large-mass DLA clusters, we have followed the strategy advocated by Tolman and Meakin [72] to improve and extend in higher dimensionalities previous off-lattice algorithms [77,78]. Directly inspired by the hierarchical on-lattice algorithms developed by Ball and Brady [62], this approach consists in constructing a collection of coarse-grained versions of the cluster at different scales. First, the cluster as seen at the coarsest scale is examined and if a jump on that scale can be taken by the diffusing particle, the jump is executed. Otherwise, one switches to the next lower scale version of the cluster in order to get more accurate information about the location of the cluster in the vicinity of the particle. This process of consulting more and more resolved approximations of the cluster continues until one reaches the lowest scale. At this level, from the knowledge of the exact location of the cluster particles, one knows whether the diffusing particle has already contacted the cluster or if it can be moved by a small distance of the order of one particle radius. After a particle has been added to the cluster, the collection of hierarchical coarse-grained versions of the DLA cluster must be updated.

In order to generate DLA clusters of slightly overlapping particles, we fix once for all the values of the overlapping parameter $\delta=0.2$. We refer the reader to Ref. [73], where the effect of this model parameter on the DLA morphological characteristics has been investigated systematically. As in our previous study of on-lattice DLA clusters in Ref. [57], we use a numerical trick to initiate the growth from the cell axis: the very first random walking particles are likely to

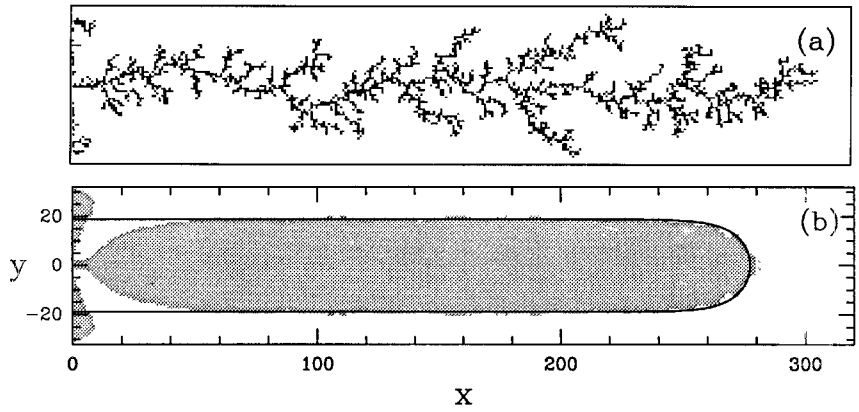

FIG. 1. (a) An off-lattice DLA cluster of mass $M=2700$ grown in a channel of width $W=64$. (b) Region of the strip with mean occupancy above the ''mean'' rate $\overline{\rho_m}=0.142$ [Eq. (5)]; 255 aggregates of the type shown in (a) were grown to obtain this repartition. The continuous line is the shape of the Saffman-Taylor analytical solution of width $\lambda=0.60$ [Eq. (1)].

stick onto a needle centered on the cell axis and the length of which is scaled on the width of the strip (practically $L_n=5W/32$). This algorithmic artifice reduces considerably the period of the selection regime [14,79–83] among DLA trees grown from the linear substrate, which is out of the scope of the present analysis. In Fig. 1(a) is shown a cluster of mass $M=2700$, grown with our off-lattice algorithm in a strip of width $W=64a$ (for the sake of simplicity we will set $a=1$ in the rest of this paper and we will express W as well as other length variables in particle size units). The mass is chosen large enough that the characteristic size of the aggregate (along $0x$) be much larger than W for the steady fractal growth regime to settle down. In practice, the criterion we use is to adapt the mass M to the value of the cell width W so that the average length of the aggregate $X_{\rm tip}>3W$; actually this provides us with an intermediate region of size larger than W where the steady fractal regime can be studied statistically [57–59].

Our statistical analysis of off-lattice DLA clusters consists in measuring the mean occupancy $\rho(x,y)$ of each site of the strip [57]. In a given strip of width W, we therefore grow N aggregates with the same total number M of particles. For each aggregate, we associate each of its particles to the site of the grid closest to it. We then count for each point of the grid how many times it has been occupied by a particle of an aggregate. The mean occupancy $\rho(x,y)$ is obtained by dividing this number by the total number N of realizations. When averaging 255 DLA clusters of the type shown in Fig. 1(a), one gets the mean occupancy distribution represented under various forms in Fig. 2. The three-dimensional representation of $\rho(x,y)$ in Fig. 2(a), as well as the contour plots in Fig. 2(b) and the mean occupancy $\rho(x,y=0)$ along the axis of the channel in Fig. 2(c) clearly show three distinct regimes. First there is some initial transient regime ($0<x<50$) where one progressively loses the influence of the initial conditions (mainly the presence of the needle) to the benefit of the growth, which settles in the center of the channel from the beginning. Then, there is a region where the cell translational invariance imposes itself on the occupancy profile ($50<x<225$); in this region the screening between the branches no longer operates and the growth has ceased. The falloff of the mean occupancy at the front zone corresponds to the active part of each pattern and to the dispersion of the tip position ($x>225$). As seen in Fig. 2(b), the overall contour plots have a finger shape that strongly resembles the set of analytical solutions [Eq. (1)] derived by Saffman and Taylor [19]. Let us note, however, that the global shape of $\rho(x,y)$ does not match the occupancy distribution of a stable viscous finger. This is obvious in Fig. 2(d) where some transverse section of the mean occupancy is shown to deviate significantly from a step profile [$\rho=1$ at the center of the cell (air) and $\rho=0$ on the edge (oil)]. Indeed, the histogram presented in this figure is an averaged transverse profile obtained by taking advantage of the translational invariance and summing over our statistical sample of 128 transverse sections in the asymptotic steady fractal regime [29,73]:

$$\overline{\rho(y)}=\sum_{x=80}^{208}\rho(x,y)/128.$$

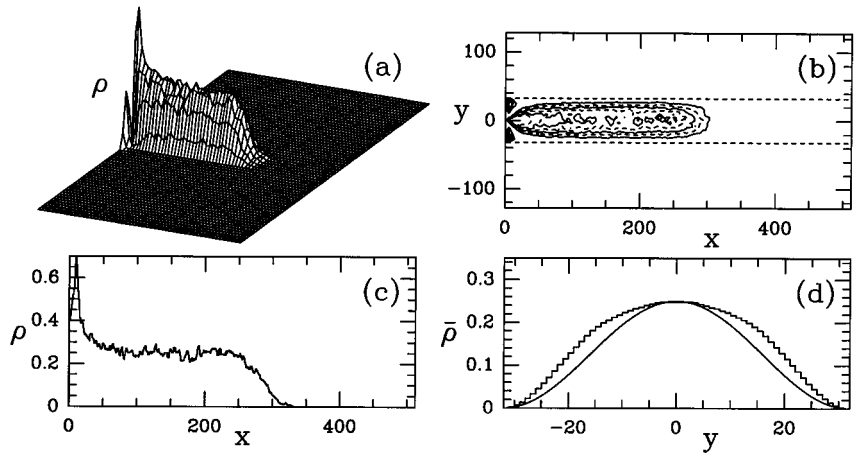

FIG. 2. Statistical analysis of off-lattice DLA clusters of mass $M=2700$ grown in a channel of width $W=64$. Our statistical sample involves $N=255$ aggregates similar to the one shown in Fig. 1(a). (a) Three-dimensional representation of the mean occupancy $\rho(x,y)$. (b) Contour plots for ρ: the levels are 0.05, 0.10, 0.15, 0.20, and 0.25 from outer to inner. (c) Histogram of the mean occupancy along the axis of the strip: $\rho(x,y=0)$. (d) Histogram of the mean transverse occupancy averaged over 128 sections across the channel: $\overline{\rho(y)}=\Sigma_{x=80}^{208}\rho(x,y)/128$. The solid line corresponds to the conjectured transverse profile $\rho_T(y)=\rho_{\max}\cos^2(\pi y/W)$ [Eq. (2)].

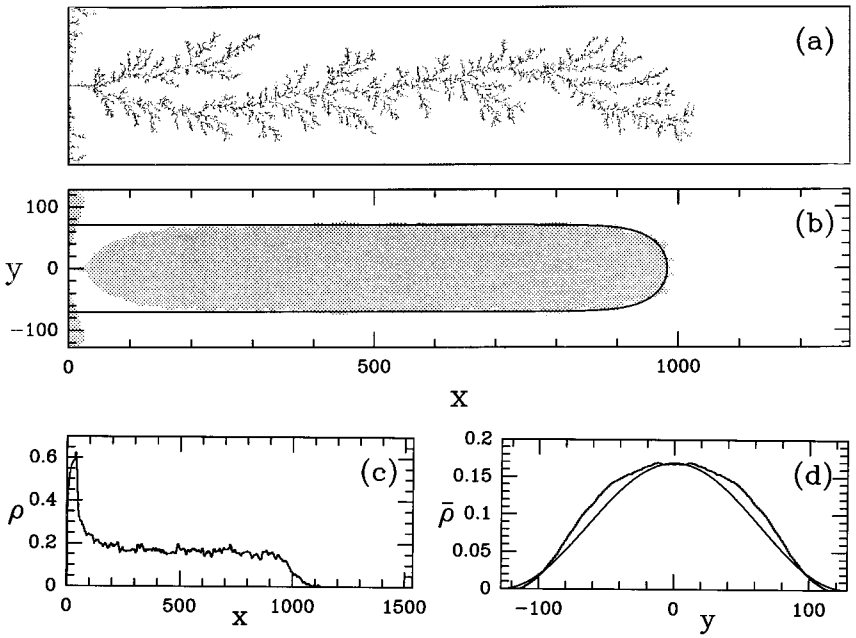

FIG. 3. Statistical analysis of $N=255$ off-lattice DLA clusters of mass $M=24\,000$ grown in a strip of width $W=256$. (a) A realization of the off-lattice DLA process. (b) The points of the cell where the mean occupancy is above the ''mean'' rate $\overline{\rho_m}=0.095$ are represented in grey. The continuous line is the shape of the ST analytical solution of width $\lambda=0.57$ [Eq. (1)]. (c) Histogram of mean longitudinal occupancy $\rho(x, y=0)$. (d) Averaged histogram of mean transverse occupancy over 512 sections across the strip in the steady fractal regime: $\overline{\rho(y)}$. The conjectured transverse profile $\rho_T(y)=\rho_{\max}\cos^2(\pi y/W)$ [Eq. (2)] is shown in solid line for comparison.

This transverse occupancy profile has a maximum $\overline{\rho_{\max}}$ at the center ($y=0$) and decreases smoothly to zero at the walls ($y=\pm W/2$). It turns out also to be different from the asymptotic profile:

$$\rho_T(y)=\rho_{\max}\cos^2(\pi y/W), \tag{2}$$

conjectured by Arneodo *et al.* [57] in a similar statistical study of on-lattice DLA clusters [see also Fig. 5(d)]. However, if according to the recipe proposed in Refs. [29, 58, and 59], one estimates the ''mean'' width of the mean occupancy by determining the points on each side of the cell axis that satisfy

$$y_m^{\pm}=\frac{1}{\overline{\rho_{\max}}}\sum_{0}^{\pm W/2}\overline{\rho(y)}, \tag{3}$$

one gets for the relative width

$$\lambda=(y_m^{+}-y_m^{-})/W \tag{4}$$

a value $\lambda=0.60\pm0.03$, which is definitely larger than the value 0.50 expected from the conjectured transverse profile in Eq. (2) (the estimate of the error bar relies upon our statistical sample of 128 transverse occupancy histograms). Let us emphasize that this definition of the relative mean width of the mean occupancy amounts to comparing $\overline{\rho(y)}$ to a step profile of the same height $\overline{\rho_{\max}}$ and the same integral. Now if one selects only the points of the strip of mean occupancy larger than the mean rate,

$$\overline{\rho_m}=\overline{\rho(y_m^{\pm})}, \tag{5}$$

namely, $\rho\geqslant14.2\%$ ($\geqslant\rho_{\max}/2$), one defines a region of large occupancy that is remarkably well fitted by the Saffman-Taylor analytical solution of relative width $\lambda=0.60$ [Eq. (1)], as shown in Fig. 1(b). Thus, one recovers the same rather striking result as originally discovered for on-lattice DLA clusters in Ref. [57] [see also Fig. 5(b)], except that the relative width λ of this mean finger is significantly larger than the value $\lambda=\frac{1}{2}$ obtained for on-lattice DLA clusters in surprising agreement with the relative width of the stable ST finger selected by surface tension [32–40]. We will spend the rest of this section discussing this apparent discrepancy.

We have repeated our statistical analysis of off-lattice DLA clusters for channels of various widths ranging from $W=16$ to 256. As illustrated in Fig. 3 for the widest cell ($W=256$), the main features observed in Figs. 1 and 2 withstand such a change in the cell size. In particular, the mean ensemble-averaged DLA profile defined from Eqs. (3) and (4) has again the shape of one member of the ST analytical solution family [Eq. (1)]; the solid line in Fig. 3(b) represents the profile of the ST finger of relative width $\lambda=0.57$. From the computation of 512 histograms of mean transverse occupancy corresponding to as many sections across the strip in the steady fractal regime ($250<x<850$), one gets the average transverse histogram shown in Fig. 3(d). Its width $\lambda=0.57\pm0.02$ is slightly smaller than the width of the average finger observed for $W=64$ in Fig. 1(b). The estimates of λ obtained for different values of W are reported in Fig. 4, as a function of $1/W$. Despite some slow decrease of λ when increasing W, it seems that for cells of width $W>100$, one does not observe any further quantitative change in the estimate of λ. Actually, λ is likely to converge towards an asymptotic limit value $\lambda=0.57\pm0.02$, which is significantly (with respect to the statistical uncertainty) larger than the asymptotic prediction $\lambda=\frac{1}{2}$ for the relative width of stable ST fingers in the limit $B\to0$.

In Fig. 4 are also reported the values of the relative width λ of the large occupancy region obtained for DLA clusters generated using the on-lattice algorithm described in Ref. [84], the lattice being parallel to the cell axis. For W ranging from 16 to 256, λ is found significantly smaller for on-lattice than for off-lattice DLA clusters. Actually, as previously pointed out by Arneodo *et al.* [57], the on-lattice data fall remarkably close to the asymptotic prediction $\lambda=\frac{1}{2}$ for the selected ST finger in the limit of zero surface tension. In

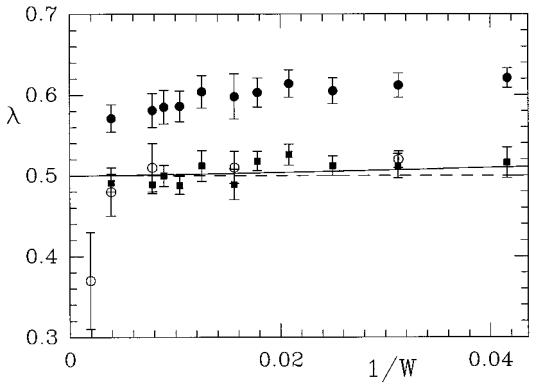

FIG. 4. The relative width λ of the large occupancy region defined from the criterion (3) and (4) vs $1/W$: ●, off-lattice simulations, $N=1000$; ○, on-lattice simulations, $N=1000$ ($W=16,32,64$), 255 ($W=128$), 480 ($W=256$), and 50 ($W=512$). The symbols ■ correspond to off-lattice simulations when defining the large occupancy region from the $0.6\overline{\rho_{\max}}$ contour lines [Eq. (6)]. The solid line corresponds to the theoretical prediction [Eq. (7)] for the relative width $\lambda_{n=0}(1/W)$ of the stable smooth ST finger with a capillary length $l_c=4a$.

order to carry out a detailed comparison between off-lattice and on-lattice growths, we summarize in Fig. 5 the results of a statistical analysis of $N=1000$ on-lattice DLA clusters of mass $M=2700$, grown in a strip of width $W=64$ in similar conditions as the off-lattice simulations shown in Figs. 1 and 2. As seen on the region of large occupancy in Fig. 5(b), its profile is still very well fitted by the shape of a ST finger, but this finger is narrower, $\lambda=0.51\pm0.02$, and therefore longer ($X_{\rm tip}\sim360$) than the off-lattice ST finger ($X_{\rm tip}\sim280$) in Fig. 1(b). This observation is a strong indication that the presence of an underlying lattice favors the growth along the lattice axis, which is parallel to the cell axis. The anisotropy induced by the lattice at a microscopic level in the sticking rule therefore imposes some preferential direction of growth at a macroscopic level [62–71]. This phenomenon becomes more and more pronounced when one considers wider and wider strips. Individual realizations evolve progressively towards dendritic fractal patterns while the region of mean occupancy becomes narrower and narrower [58] as one can guess from Fig. 4 where the relative width of the mean finger obtained for $W=512$ ($N=50$), $\lambda=0.37\pm0.06$, is definitely smaller than the asymptotic limit $\lambda=\frac{1}{2}$ for isotropic fingers. At this point, we refer the reader to a previous study of anisotropic Laplacian growths by Arneodo *et al.* [59], where this anisotropy-induced morphological transition from DLA to dendritic patterns was quantitatively understood by analogy with the anisotropy-induced crossover known for stable smooth fingers from isotropic ($\lambda=\frac{1}{2}$) to needlelike ($\lambda=0$) ST patterns [21,85–98]. As originally pointed out in Ref. [57], the histogram of mean transverse occupancy computed for on-lattice DLA clusters [Fig. 5(d)] has a shape that is hardly distinguishable from $\rho_T(y)=\rho_{\max}\cos^2(\pi y/W)$ [Eq. (2)]. This might be pure coincidence. Let us note that this is no longer the case in the crossover regime towards dendritic growth as discussed in Ref. [59].

What seems to happen for off-lattice simulations is therefore rather different from on-lattice simulations [99]. One does not observe the crossover to dendritic patterns, which is a strong indication that our off-lattice DLA clusters are isotropic fractal aggregates. Moreover, as reported in Fig. 6, when investigating the evolution of the mean transverse occupation histogram for wider and wider strips, the rescaled transverse profile $\overline{\rho/\rho_{\max}}$ converges to an asymptotic profile, when plotted versus y/W, which is different from the conjectural profile given by Eq. (2). As seen in Fig. 3(d), this analytical profile inspired from the ensemble-averaged on-lattice DLA clusters [57] does not account precisely for the effect of the walls on the actual confinement of the growth in the central part of the strip. This explains the discrepancy obtained when estimating the relative widths of the large occupancy region for on- and off-lattice DLA clusters. Using Eqs. (3) and (4) to define this region, this amounts to selecting the $\overline{\rho_m}=0.5\overline{\rho_{\max}}$ contour line for on-lattice DLA clusters as a consequence of the specific $\cos^2(\pi y/W)$ shape of the

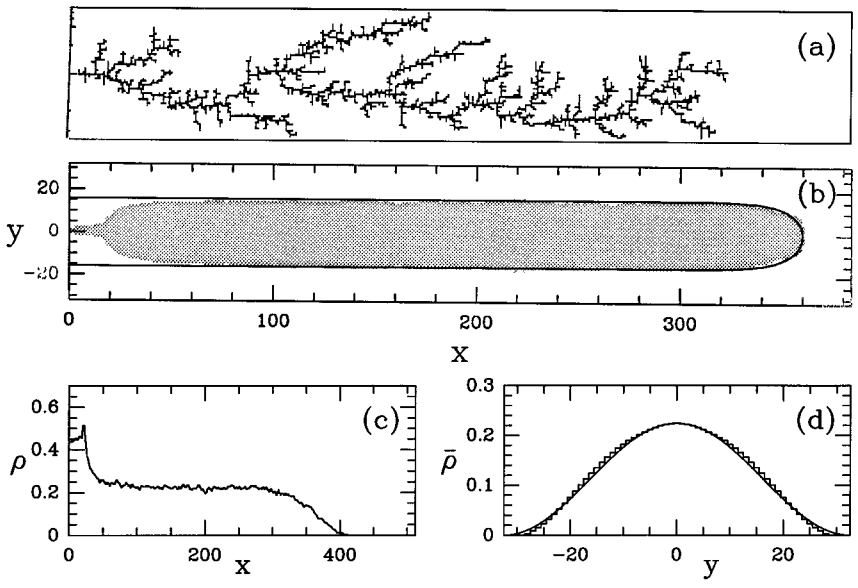

FIG. 5. Statistical analysis of $N=1000$ on-lattice DLA clusters of mass $M=2700$ grown in a strip of width $W=64$. (a) A realization of the on-lattice DLA process. (b) The points of the cell where the mean occupancy is above the average rate $\overline{\rho_m}=0.123$ ($\simeq\overline{\rho_{\max}}/2$) are presented in gray. The solid line is the shape of the ST analytical solution of width $\lambda=0.51$ [Eq. (1)]. (c) Histogram of mean longitudinal occupancy $\rho(x,y=0)$. (d) Averaged histogram of mean transverse occupancy over 128 sections ($x\in[100,228]$) across the strip in the steady fractal regime: $\overline{\rho(y)}$. The conjectured profile $\rho_T(y)=\rho_{\max}\cos^2(\pi y/W)$ [Eq. (2)] is shown in solid line for comparison.

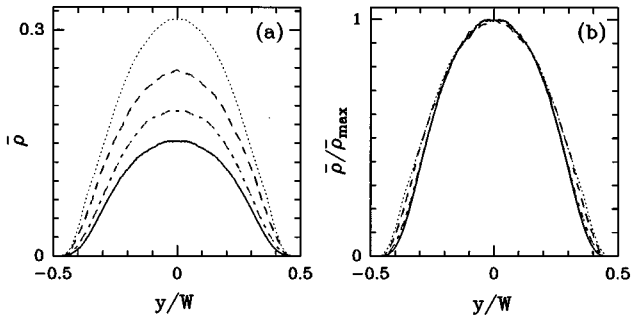

FIG. 6. Evolution of the histogram of mean transverse occupancy for off-lattice DLA simulations in a linear strip of increasing width. (a) $\overline{\rho}$ vs y/W: $W=32$, 64, 128, and 256 from top to bottom. (b) $\overline{\rho}/\overline{\rho}_{\max}$ vs y/W.

mean transverse occupancy profile [Fig. 5(d)]. One then deduces that the region of large occupancy defined by the points of the strip with an occupancy rate above the average $\overline{\rho} \geqslant \overline{\rho}_{\max}/2$ has a relative width $\lambda=0.5$. This is no longer true for off-lattice DLA clusters whose asymptotic mean transverse profile has a different shape and therefore a relative width significantly larger than $\frac{1}{2}$ if one uses the same arbitrary criteria as for on-lattice simulations. But, as shown in Fig. 4, if one considers as an alternative definition for the limit of the region of large occupancy the $0.6\overline{\rho}_{\max}$ contour line, one gets estimates of the relative width λ that are quite similar to those obtained for on-lattice DLA clusters, namely, $\lambda=0.50$ for strips of width ranging from $W=16$ to 256. Moreover, as illustrated in Fig. 7(e), the so-defined large occupancy region is again remarkably well fitted by the analytical shape of the stable ST finger. Thus, by considering the points in the strip with an occupancy rate above some critical proportion of the maximum occupancy rate (at the center of the channel), which turns out to be surprisingly close to the magic proportion,

$$\overline{\rho}(x,y) \geqslant (1/\phi)\overline{\rho}_{\max}(x,y=0), \tag{6}$$

where $\phi=1.618$ is the golden mean, one recovers statistically the shape of the stable ST finger selected by surface tension. Therefore, these results once more confirm the deep connection between viscous fingering and DLA growth. What is really astonishing here is that going from the stable finger to unstable fractal patterns, the selection of a solution seems to survive its instability [57]. Underlying each DLA realization there is, as a statistical guide, a region of large occupancy that has the shape and the relative width of the corresponding stable ST finger. In that respect, our results indicate that the role of the viscous finger capillary length scale is played by the particle size a for DLA clusters. This is confirmed quantitatively in Fig. 4, where our set of data for the relative width λ of the ensemble-averaged off-lattice DLA patterns is compared with the asymptotic theoretical prediction for the branch $\lambda_{n=0}(B)$ of stable fingers selected by surface tension [34–40]:

$$\lambda_{n=0}(B) \approx \frac{1}{2} + 2^3\left(\frac{\pi}{7}\right)^{4/3} B^{2/3}. \tag{7}$$

When identifying the capillary length l_c to a few particle sizes ($l_c < 4a$) in the expression of the dimensionless parameter $B=(1/12\pi^2)(l_c/W)^2$, Eq. (7) provides a remarkable fit for the numerical data.

In Fig. 7 are also shown the regions of the strip that are respectively delimited by different contour lines from $0.2\overline{\rho}_{\max}$ to $0.8\overline{\rho}_{\max}$. It is clear that the contour lines corresponding to small occupancy [Figs. 7(a) and 7(b)] significantly deviate from the ST finger shape (of corresponding relative width), which displays a rather flat tip for large λ that is not reproduced by our ensemble-averaged off-lattice DLA patterns. The comparison for the highest level curves of large occupancy [Figs. 7(f) and 7(g)] is made difficult by some lack of statistical convergence to a smooth finger profile. But from a careful examination of the $0.4\overline{\rho}_{\max}$, $0.5\overline{\rho}_{\max}$, and $0.6\overline{\rho}_{\max}$ contour lines in Figs. 7(c), 7(d), and 7(e), respectively, it is rather delicate to decide whether the $0.6\overline{\rho}_{\max}$ level curve plays a privileged role in the sense that it may be the only one with an exact ST shape. We do not think that there is hope of answering this question from extensive numerical simulations.

So far, we have mainly considered the region of the mean occupancy profile, which is invariant by translation and which corresponds to a region where the growth is no longer active. As shown in Fig. 8(a), the histogram of mean longitudinal occupancy $\rho(x,y=0)$ is quite flat in this region up to some fluctuations due to finite-size effects. When increasing the mass M of the DLA clusters, this inactive zone progressively invades the cell; indeed, when scaled on W, the mean length of the cluster x_F/W turns out to be proportional to its mass M (x_F denotes the position of the active front). In the front zone, the falloff of $\rho(x,y=0)$ accounts for the dispersion of the tip position of each DLA realization. As shown in Fig. 8(c), the width of this active zone increases during the growth with a dependence $\Delta_F/W \sim (x_F/W)^{1/2}$, which is quite consistent with the behavior observed for on-lattice DLA clusters [57]. As originally pointed out in Ref. [57], this can be understood if one considers the growth process, on the scale W, as the successive addition of n independent bunches of a fixed number of particles having different configurations and thus different lengths so that the dispersion of the tip position be proportional to $\sqrt{n}$.

B. Mean-field diffusion-limited aggregation

A first attempt to establish a mean-field theory for DLA growth goes back to the pioneering work of Witten and Sander [50]. In their original paper, these authors raised the issue of a general continuous formulation for the time development of some ensemble average of DLA clusters. They proposed the following equations:

$$\partial\rho/\partial t = \nabla^2 u, \tag{8a}$$

$$\partial\rho/\partial t = u(\rho + a^2\nabla^2\rho), \tag{8b}$$

where ρ and u are the mean densities for ''aggregates'' and ''walkers,'' respectively, and a is the lattice spacing. Equation (8a) is nothing more than the conservation of mass. Equation (8b) accounts for the growing rule of the ''aggregate'' field. Unfortunately, as pointed out by Hakim and coworkers [42], these equations are not correct in channel ge-

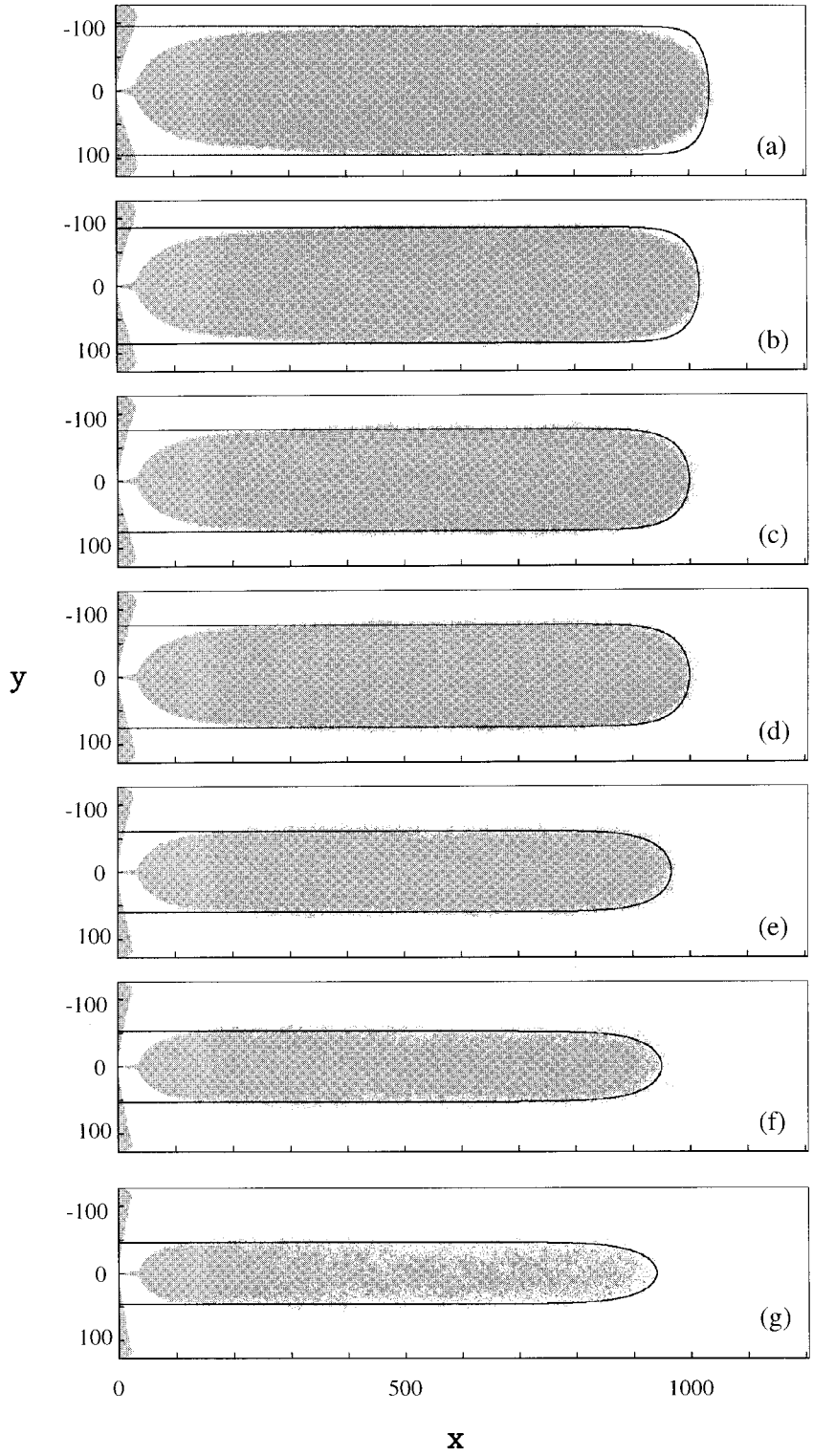

FIG. 7. Statistical analysis of $N=1000$ off-lattice DLA clusters of mass $M=24\,000$ grown in a strip of width $W=256$. In gray are represented the points of the cell where the mean occupancy is above $0.2\overline{\rho}_{\max}$ (a), $0.3\overline{\rho}_{\max}$ (b), $0.4\overline{\rho}_{\max}$ (c), $0.5\overline{\rho}_{\max}$ (d), $0.6\overline{\rho}_{\max}$ (e), $0.7\overline{\rho}_{\max}$ (f), and $0.8\overline{\rho}_{\max}$ (g). The solid lines correspond to the ST finger analytical solution of relative width $\lambda=0.73$ (a), 0.67 (b), 0.61 (c), 0.56 (d), 0.49 (e), 0.41 (f), and 0.31 (g).

ometry since there is no steady solution evolving at constant velocity. Indeed, the longitudinal profile of ρ displays a $1/x^2$ power-law behavior, which explains the interface acceleration.

In order to remedy the insufficiencies of the Witten and Sander mean-field equations in such a way that they provide some understanding of the ensemble-averaged on-lattice DLA patterns found by Arneodo *et al.* [57], Brener, Levine, and Tu [60] (see also Ref. [100]) have recently proposed some modification to Eq. (8). This modification consists in replacing ρ by ρ^γ in Eq. (8b):

$$\partial\rho/\partial t=\nabla^2 u, \tag{9a}$$

$$\partial\rho/\partial t=u(\rho^\gamma+a^2\nabla^2\rho). \tag{9b}$$

As argued in Ref. [60], taking γ greater than 1 is a way, among others, to introduce a cutoff in the growth rate at

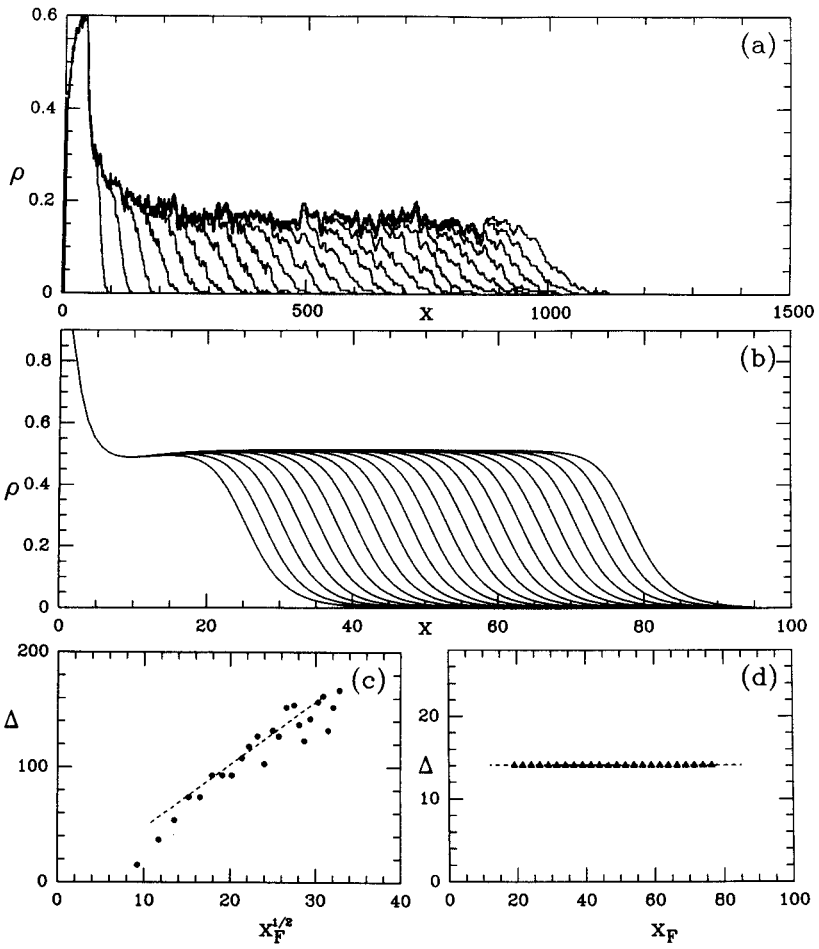

FIG. 8. (a) Statistical analysis of $N=255$ off-lattice DLA clusters grown in a channel of width $W=256$. The histogram of mean longitudinal occupancy is shown at different stages of growth: $M=1000n$, for $n=1,2,\ldots,24$. (b) Longitudinal profile of the ''aggregate'' ρ field as computed with the MFT equations (9)–(12) at different stages of growth: $t=5n$, for $n=1,2,\ldots,22$; the model parameters are $\varphi=1$, $\gamma=2$, $a=1$, and $W=20$. (c) Width of the active front zone Δ_F vs $x_F^{1/2}$, where x_F is the location of this front, extracted from the off-lattice DLA simulations. (d) Δ_F vs x_F for the MFT calculations.

small density that will mimic the fact that in the DLA model, growth cannot occur with an infinitesimal fluctuation of ρ. Therefore, as compared to Eq. (8), Eq. (9) is likely to account for the discrete character of the DLA model, where the diffusing particle only sticks to the aggregate when it overlaps a cluster particle. Moreover, since DLA growth imposes working with constant flux, i.e., with a finite slope of the u field at infinity, the presence of this cutoff prevents any arbitrarily small fluctuation in front of the growing front to start developing and thereby keeps the front from accelerating indefinitely.

Encouraged by the very promising results obtained by Brener, Levine, and Tu [60], we have reproduced in Fig. 9 the results of some simulations that demonstrate clearly the capability of the mean-field Eq. (9) to display steady-state growth in a channel geometry. On the lateral boundaries of the strip, we have imposed Neuman conditions for the u field and Dirichlet condition for the ρ field:

$$\left.\frac{\partial u}{\partial y}\right|_{y=\pm W/2}=0 \tag{10}$$

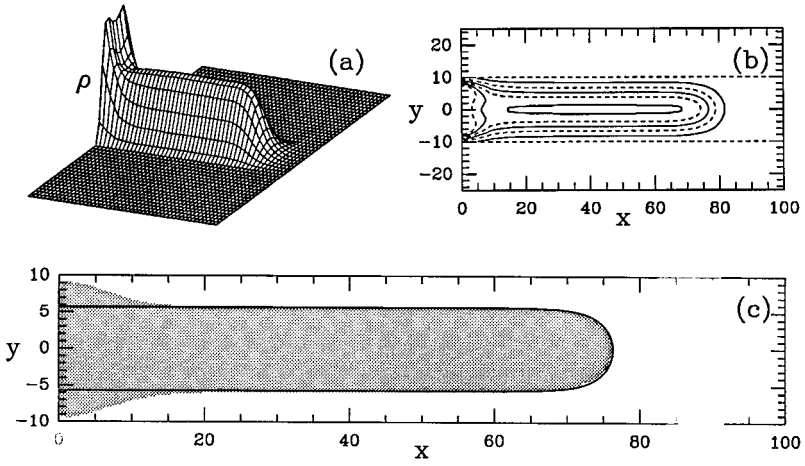

FIG. 9. Mean-field calculations of the aggregate field distribution in a channel geometry with the model parameters: $\varphi=1$, $\gamma=2$, $a=1$, and $W=20$. (a) Three-dimensional representation of $\rho(x,y)$. (b) Contour plots for ρ, the levels are 0.10, 0.20, 0.30, 0.40, and 0.50 from the outer to the inner. (c) In gray are shown the points of the channel where the ρ density is above the average rate $\overline{\rho_m}=0.276$. The continuous line is the shape of the ST analytical finger of width $\lambda=0.55$.

and

$$\rho|_{y=\pm W/2}=0. \tag{11}$$

At the far end extremity of the strip, we have fixed the flux of the walkers:

$$\left.\frac{\partial u}{\partial x}\right|_{x=L}=\varphi. \tag{12}$$

The numerical procedure used to simulate Eq. (9) is in the spirit of the quasistatic approximation that underlies the derivation of these mean-field equations [60]. Given an initial distribution for ρ, one solves the spatially forced Poisson's equation:

$$(-\nabla^2+\rho^{\gamma}+a^2\nabla^2\rho)u=0. \tag{13}$$

Then, from the distribution of u, one computes $\partial\rho/\partial t$ from Eq. (9a), and the ρ field can be advanced in time. In order to account for the symmetry about the center of the channel inherent to the averaging over many DLA clusters, one can easily enforce this symmetry in the mean-field simulations by starting from an initial condition for the ρ field, which is invariant under this symmetry. The evolution under Eq. (9) actually preserves this symmetry.

The mean-field approach proposed by Brener, Levine, and Tu [60] depends, *a priori*, upon four parameters: the flux φ, the cutoff exponent γ, the lattice spacing a, and the channel width W. However, if one rescales the time and the u field as

$$t=\varphi^{-1}\tilde{t}, \quad u=\varphi\tilde{u}, \tag{14}$$

one can fix the flux,

$$\varphi=1, \tag{15}$$

without modifying Eq. (9). Let us note that fixing the flux to 1 is quite reasonable since it amounts to identifying the mass to the time in the discrete DLA model. Now one can further rescale time, space, and the ρ and u fields in the following way:

$$t=a^{\gamma/2-2}\hat{t}, \quad x=a^{\gamma/2}\hat{x}, \quad y=a^{\gamma/2}\hat{x},$$

$$\rho=a^{-2}\hat{\rho}, \quad u=a^{\gamma/2}\hat{u}, \tag{16}$$

which allows us to keep $\varphi=1$ and to fix the value of the lattice spacing to unity:

$$a=1. \tag{17}$$

In the simulations presented in this section, the width W of the channel will therefore be expressed in lattice spacing units. Let us note at this point that the two rescaling transformations (14) and (16) do affect the aggregate field ρ; this remark will be of fundamental importance in the following when we will compare the MFT predictions to the ensemble-averaged DLA patterns.

We have thus performed simulations for various values of γ and W. We have tested the convergence of our numerical code according to the spatial resolution in both the x and y directions. Most of the results reported below correspond to lattices of size $L\times 40$, where $L\in[50,200]$ is adjusted according to the values of the parameters γ and W. As seen in Fig. 9, for the parameter values extracted from Ref. [60], namely, $\gamma=2$ and $W=20$, the ρ density distribution displays similar characteristics to the mean occupancy of off-lattice DLA clusters in Figs. 1, 2, and 3. After some initial transient period, the active front zone leaves an inactive ρ profile behind it, which displays translational invariance. This is seen clearly both on the contour plots in Fig. 9(b), which have a finger shape, and on the longitudinal ρ profile in Fig. 8(b), which is constant before the falloff to zero ahead of the growth. From the transverse ρ profile shown in Fig. 10(a), we have represented in grey in Fig. 9(c) the points of the channel with a density that exceeds the average rate $\overline{\rho_m}$ defined in Eqs. (3) and (5). Very much like the ensemble-averaged off-lattice DLA patterns in Figs. 1(b) and 3(b), the boundary of this region of large occupancy is very well fitted by the analytical ST solution of relative width $\lambda=0.55$ (note that very much like for the ensemble-averaged DLA patterns, not all the contour plots have the ST finger shape). This is without any doubt a very encouraging observation. Nevertheless, in order to conclude as to the relevance of this mean-field theory, one needs to proceed to a more quantitative comparison.

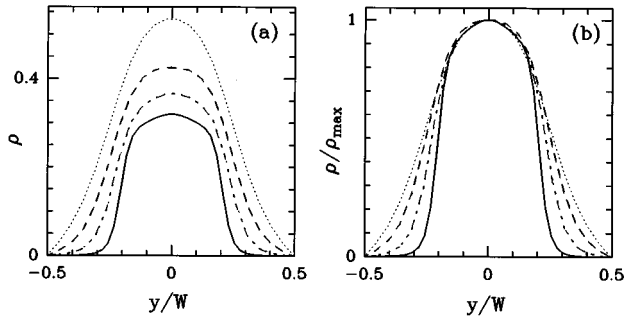

FIG. 10. Mean-field calculations of the transverse profile of the ρ field with the model parameters: $\varphi=1$, $\gamma=2$, $a=1$. (a) ρ vs y for channels of width $W=32$, 64, 128, and 256 from top to bottom. (b) $\rho/\rho_{\max}$ vs y/W.

In Fig. 10 are shown the transverse ρ profiles computed with $\gamma=2$ for different values of the channel width W. Two main features characterize the evolution of these profiles. First, the maximum value $\rho_{\max}$ at the center of the channel decreases when increasing W [Fig. 10(a)]; we will come back to this point for the fractal analysis carried out in Sec. II C. Then, the shape of the transverse ρ density evolves from a smooth to a steeper profile [Fig. 10(b)]; the intermediate region between the large occupancy region in the center of the channel and the small occupancy regions near the walls becomes narrower with increasing W. As shown in Fig. 11, the relative width λ of the large occupancy region defined as in Fig. 9(c) actually decreases from values that are significantly larger than $\frac{1}{2}$ for narrow strips ($\lambda=0.55\pm0.01$ for $W=20$) to values that approach $\frac{1}{2}$ for wider strips ($\lambda=0.52\pm0.01$ for $W=60$). Indeed, as illustrated in Fig. 10(b), the rescaled mean transverse profile $\overline{\rho/\rho_{\max}}(y/W)$ does not seem to converge to any asymptotic profile as observed numerically for the ensemble averages of both on-lattice and off-lattice DLA patterns (this observation does not preclude the possibility of some convergence for very wide strips of

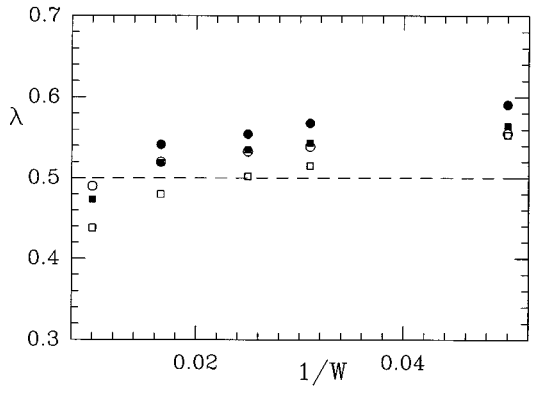

FIG. 11. Mean-field calculations of the relative width λ of the region of large occupancy defined as in Fig. 9(c), for various values of the cutoff parameter γ. The model parameters are $\varphi=1$ and $a=1$. λ is plotted vs $1/W$. The symbols correspond to $\gamma=1.2$ (●), 1.6 (■), 2 (○), and 5 (□).

width W much larger than those achieved with our computer capabilities). Consequently, there is no indication that the relative width λ of the large occupancy region defined from the criterion given by Eqs. (3) and (4) as well as from any contour line converges to the asymptotic value $\lambda=\frac{1}{2}$ predicted for the stable ST finger in the limit of zero surface tension [33–40]. There is no evidence that λ converges to any finite value either larger or smaller than $\frac{1}{2}$.

In Fig. 12, we have investigated the behavior of the transverse ρ profile when varying the cutoff parameter γ for a fixed value $W=64$ of the width of the channel. When increasing γ, $\rho_{\max}$ increases [Fig. 12(a)] while, as seen in Fig. 12(b), the rescaled mean transverse occupancy histogram evolves towards a step-function profile characteristic of stable fingers. This observation is quite consistent with the remark of Brener, Levine, and Tu [60] that in the limiting case where $\gamma\to+\infty$ and $a\to0$ (or $W\to+\infty$), the MF equations become exactly the Saffman-Taylor problem at zero surface tension. For each of the γ values considered in Fig. 12, we have further analyzed the dependence of the transverse ρ profile as a function of W. At a qualitative level, whatever the value of γ, one recovers the same characteristic features as observed for $\gamma=2$ in Fig. 10. At a quantitative level, we have reported in Fig. 11 the estimate of the relative

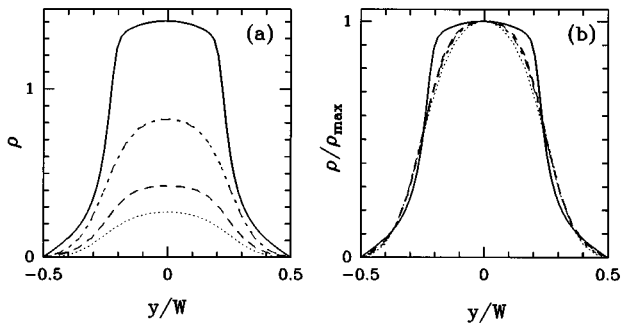

FIG. 12. Mean-field calculations of the transverse profile of the ρ field with the model parameters: $\varphi=1$, $a=1$, $W=64$. (a) ρ vs y for $\gamma=1.2$, 1.6, 2, and 5 from bottom to top; (b) $\rho/\rho_{\max}$ vs y/W.

width λ of the large occupancy region ($\rho>\overline{\rho_m}$) versus $1/W$. For each value of γ, λ systematically decreases when increasing W. For a given value of W, λ apparently decreases when increasing γ: for the mean transverse profiles shown in Fig. 12 for $W=60$, one obtains precisely $\lambda=0.54$ ($\gamma=1.2$), 0.52 ($\gamma=1.6$), 0.52 ($\gamma=2$), and 0.48 ($\gamma=5$).

As pointed out by Brener, Levine, and Tu [60] in their original paper, this mean-field approach has an intrinsic problem that, to our knowledge, is not yet understood: it fails to reproduce the spreading of the active front zone during DLA growth [57]. In Fig. 8, the evolution of the longitudinal profile of the aggregate field in the mean-field theory [Fig. 8(b)] is compared to the histogram of mean longitudinal occupancy in DLA simulations [Fig. 8(a)]. As shown in Fig. 8(d), the width of the front zone Δx_F computed with the mean-field equations does not display any time dependence, a result that is in contradiction with the scaling behavior $\Delta x_F\sim M^{1/2}\sim x_F^{1/2}$ observed in Fig. 8(c) for the DLA simulations. This failure is, without any doubt, one of the main weaknesses of the mean-field approach proposed (so far) for diffusion-limited aggregation.

C. Fractal analysis

The next step of our study is to demonstrate that the fractal dimension of the DLA clusters can be extracted from the W dependence of the mean occupancy distribution. As previously pointed out [57–59], from the translational invariance of this distribution along the growth axis, one deduces readily that the mass has a one-dimensional component in the $0x$ direction that behaves as

$$M_L(x)\propto x^{D_L} \quad \text{with} \quad D_L=1, \tag{18}$$

where D_L is the longitudinal partial dimension (consistently we have seen in Fig. 8 that the position of the growing front behaves as $x_F\propto M$). Obviously, the geometrical fractality of the patterns has to come from the direction perpendicular to the channel axis [82,101]. The computation of the area of the mean transverse occupancy profile as a function of the width of the channel gives the transverse partial dimension D_T:

$$A(W)=M_T(W)\propto W^{D_T}, \tag{19}$$

and in turn, from the trivial behavior in the longitudinal direction [Eq. (18)], the fractal dimension D_F is [102]

$$D_F=D_T+1. \tag{20}$$

From the mean transverse occupation histograms computed from on-lattice and off-lattice simulations, for various channel widths W ranging from 16 to 256, we have calculated the area $A(W)$ of each histogram and we have plotted in Fig. 13 $A(W)W\propto W^{D_F}$ as a function of W in a log-log representation. Both the on-lattice and off-lattice data remarkably fall on a straight line; the dashed lines in Fig. 13 are lines of slope 1.66 ± 0.01, which provide an excellent fit of the two sets of data. One thus gets a value of the fractal dimension,

$$D_F=1.66\pm0.01, \tag{21}$$

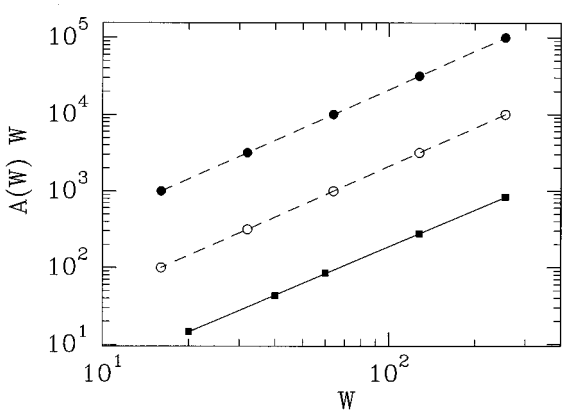

FIG. 13. Estimate of the fractal dimension D_F of DLA clusters from the computation of the W dependence of the area $A(W)$ of the mean transverse occupancy histogram. $A(W)W$ is plotted as a function of W in logarithmic scales. The dashed lines correspond to straight lines of slope $\frac{5}{3}$. Off-lattice (●) and on-lattice (○) simulations are compared to mean-field theory calculations (■) of the transverse ρ profile for the parameter values $\varphi=1$, $\gamma=2$, and $a=1$. The solid line corresponds to a fractal dimension $D_F=1.58$.

for both on-lattice [57,59] and off-lattice DLA clusters that matches perfectly the theoretical prediction [103–105] $D_F=(d^2+1)/(d+1)$ $(=\frac{5}{3})$ derived from some mean-field scaling arguments (see also Refs. [106,107]) applied to diffusion-limited aggregation in dimension $d(=2)$. Let us note that this estimate [Eq. (21)] lies between previous box-counting measurements of the fractal dimension $D_F=1.63\pm0.03$ of off-lattice DLA clusters grown in open circular geometry [74,75,108–110] and the well-known value $D_F=1.71\pm0.02$ obtained from the evolution of the radius of gyration [50,51,108,109]. This discrepancy might also indicate some morphological difference between DLA patterns grown in confined or in open geometry. One cannot also exclude the possibility of some weak multifractal departure from statistical homogeneity [111].

In Fig. 13 are also reported the results obtained from the W dependence of the transverse profile of the aggregate ρ field computed with the mean-field equations (9), (10), and (11) for the parameter values $\varphi=1$, $\gamma=2$, and $a=1$. The data again fall nicely on a straight line but the slope, $D_F=1.58\pm0.01$, is significantly smaller than the value $\frac{5}{3}$ obtained in the DLA simulations. In Fig. 14 are shown the results of a more systematic investigation of the fractal dimension D_F when varying the cutoff parameter γ. Contrary to what was suggested by Brener, Levine, and Tu [60], D_F is sensitive to the value of γ. As shown in Fig. 14(b), the $D_F(\gamma)$ curve is likely to present a minimum for a value γ^* surprisingly close to the value $\gamma=2$ (quadratic term). Since this minimum is smaller than $\frac{5}{3}$, this means that there exist two values of γ for which the mean-field equations account for the fractal dimension observed in the DLA simulations, namely, $\gamma\sim1.6$ and 4.2. But unfortunately, as seen in Fig. 15 for $\gamma=1.6$, when the mean-field theory predicts the right fractal dimension, i.e., the actual W dependence of the area of the mean transverse occupancy profile, it dramatically fails to reproduce the exact shape of this transverse profile. Indeed, the transverse ρ profile has a much steeper profile for $\gamma=1.6$ (and an even more pronounced steplike profile for $\gamma=4.2$, as previously discussed) than the numerical profiles computed with either the on-lattice or the off-lattice DLA algorithms. This is the demonstration that when pushing the comparison beyond some (spectacular) qualitative agreement, the mean-field theory, as formulated in Eq. (9), actually presents some severe deficiencies with respect to the modeling of ensemble-averaged DLA patterns.

To conclude this section, let us remark that what gives the value of the fractal dimension $D_F=\frac{5}{3}$ is mainly the W dependence of the height $\rho_{\max}$ of the mean transverse occupancy. From the definitions (3) for on-lattice DLA clusters or (6) for off-lattice DLA clusters, of the region of large occupancy, the area of the transverse occupancy profile is equal to the area of a step function profile of width λW and height $\rho_{\max}$:

$$A(W)=\rho_{\max}\lambda W\propto W^{D_T}. \tag{22}$$

Since we have seen in Fig. 4 that λ is practically equal to 0.5, up to terms of order $(1/W)^{4/3}$, one deduces from Eq. (22) that

$$\rho_{\max}\propto W^{D_T-1}\propto W^{-1/3}. \tag{23}$$

We have checked this scaling law with a good accuracy for both the on-lattice [57,59] and off-lattice DLA simulations. This scaling law is also rather well verified by the mean-field numerical results for $\gamma=1.6$ and 4.2. This can be understood by the fact that, despite the uncertainty concerning the existence of an asymptotic limit value, the relative width λ does

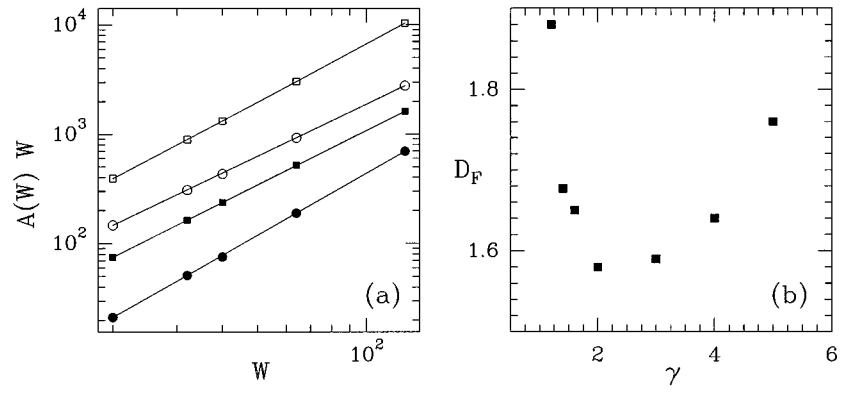

FIG. 14. Mean-field estimate of the fractal dimension D_F of DLA patterns (see Fig. 13) as a function of the cutoff parameter γ. (a) $A(W)W$ vs W in logarithmic scales; the symbols have the same meaning as in Fig. 11: $\gamma=1.2$ (●), 1.6 (■), 2 (○), and 5 (□); the solid lines correspond to linear regression fit estimate of D_F. (b) D_F vs γ.

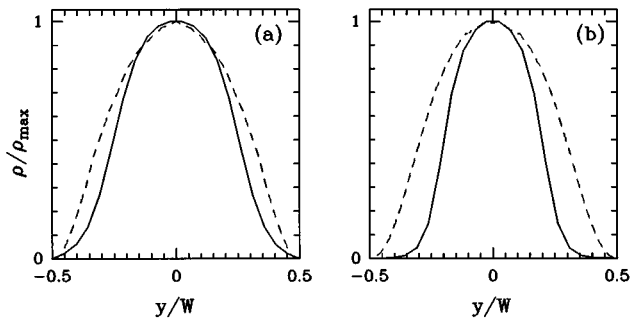

FIG. 15. Comparison of the shape of the mean transverse occupancy profile for off-lattice DLA clusters (---) with the prediction of the mean-field equation (9) (—) for the parameter values $\varphi=1$, $\gamma=1.6$, and $a=1$. (a) $W=64$; (b) $W=128$.

not vary too much when increasing the width of the strip from $W=16$ to 128 as reported in Fig. 12.

III. SECTOR GEOMETRY

A. Off-lattice DLA simulations

To conduct DLA simulations in sector geometry, we have mainly used the efficient off-lattice algorithm designed in a previous work for simulating DLA growth in circular geometry [73–75]. Initially a seed particle is located at the origin and the diffusing particles are launched at a random position from a circle of radius $r_{\max}+l$, where $r_{\max}$ is the maximum radius of the growing cluster and l has a value of a few particle diameters (practically $l=3a$). Then, in order to allow the particle to take large jumps, we have followed the very efficient strategy of hierarchical off-lattice algorithms as described in Sec. II A. According to standard practice [50,51], we have introduced an escape circle of radius $r_c=4r_{\max}$, beyond which the diffusing particle is lost. The sticking rule requires some overlap of the diffusing particle with the cluster, as characterized by an overlap parameter δ where $0\leqslant\delta\leqslant1$; as defined in Sec. II A, small δ values correspond to slight overlappings. In this section, we will mainly consider sector-shaped cells of angle $\theta_0=2\pi/2p$. This will allow us to avoid the very time consuming reflection problem on the side walls of the wedge [73]. Indeed, we just have to run the off-lattice algorithm in circular geometry, letting the particle diffuse from one sector to the next until it sticks to the cluster. Then, instead of sticking this particle at its arrival site only, we also stick a particle at each of its symmetric sites in the other $2p-1$ sectors. In this way, we will simultaneously grow $2p$ identical clusters in $2p$ complementary wedges of sector angle $\theta_0=\pi/p$. For wedges of arbitrary angle θ_0, we will alternatively proceed to the computation of the exact position of the diffusing particle after each reflection on the side walls. In Figs. 16(a) and 16(b) are shown two DLA clusters of mass $M=2000$ and 12 000, grown using this hierarchical off-lattice algorithm in two wedges of respective angle $\theta_0=30°$ and 120°.

As in linear geometry, our statistical analysis of off-lattice DLA clusters in a wedge consists in measuring the mean occupancy $\rho(r,\theta)$ of each site of the cell, where $\theta\in[-\theta_0/2,\theta_0/2]$. In a given wedge of angle θ_0, we therefore grow N aggregates with the same total number M of particles. Since the local width of the cell $W=r\theta_0$ increases during the growth, for each θ_0 we thus need to investigate several values of M in order to characterize the unsteadiness of this nonequilibrium dynamical process. When averaging over 2000 DLA clusters of the type shown in Fig. 16(a), we obtain the mean occupancy distribution represented under various forms in Fig. 17. This distribution is typical of ensemble-averaged DLA patterns at some early stage of growth in a small-angle wedge. The contour plots in Fig. 17(b) have a well-defined finger shape of fixed relative width λ. As seen on the mean azimuthal occupancy histograms $\rho(r=R,\ \theta)$ for various values of R in Fig. 17(d), the mean occupancy histogram in Fig. 17(a) is maximum along the bisector ($\theta=0$). Again, most of the growth is concentrated in the central part of the cell. Moreover, beyond some initial transient regime in the inner region of the wedge (close to the apex where the growth is strongly affected by finite-size effects), the mean radial occupancy histograms clearly decrease as a power law ($\theta=0$) when moving away from the apex, as shown in Fig. 17(c). This rarefaction comes with some spreading of the overall occupancy histogram in Fig. 17(a), which is a characteristic feature of DLA growth in an open sector geometry. In this intermediate inactive region, which precedes the falloff in the active front zone, the mean azimuthal occupancy histograms computed at different radii R can be rescaled onto a unique profile as illustrated in Fig. 18(a). This allows us to define a mean angular relative width for the ensemble-averaged DLA patterns:

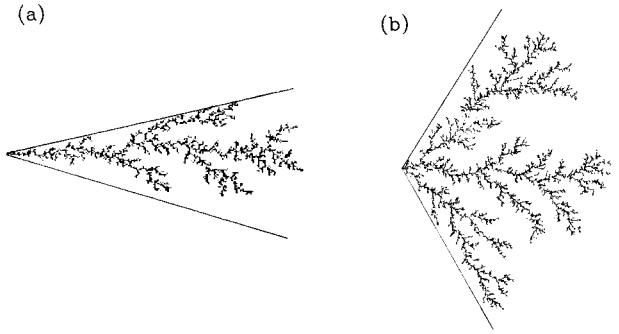

FIG. 16. Off-lattice DLA clusters grown in a wedge of angle θ_0. (a) $\theta_0=30°$; $M=2000$; (b) $\theta_0=120°$; $M=12\,000$.

$$\lambda(r)=\frac{\theta^{+}(r)-\theta^{-}(r)}{\theta_0}, \tag{24}$$

where $\theta^{\pm}(r)$ on each side of the bisector ($\theta=0$) can be defined according to either a criterion similar to Eq. (3) for on-lattice DLA simulations in a channel,

$$\theta^{\pm}(r)=\frac{1}{\rho_{\max}(r,\theta=0)}\sum_{-\theta_0/2}^{+\theta_0/2}\rho(r,\theta), \tag{25}$$

or a criterion in the spirit of Eq. (6) deduced from off-lattice DLA simulations in linear geometry:

$$\rho(r,\theta^{\pm}(r))=\frac{1}{\phi}\,\rho(r,\theta=0). \tag{26}$$

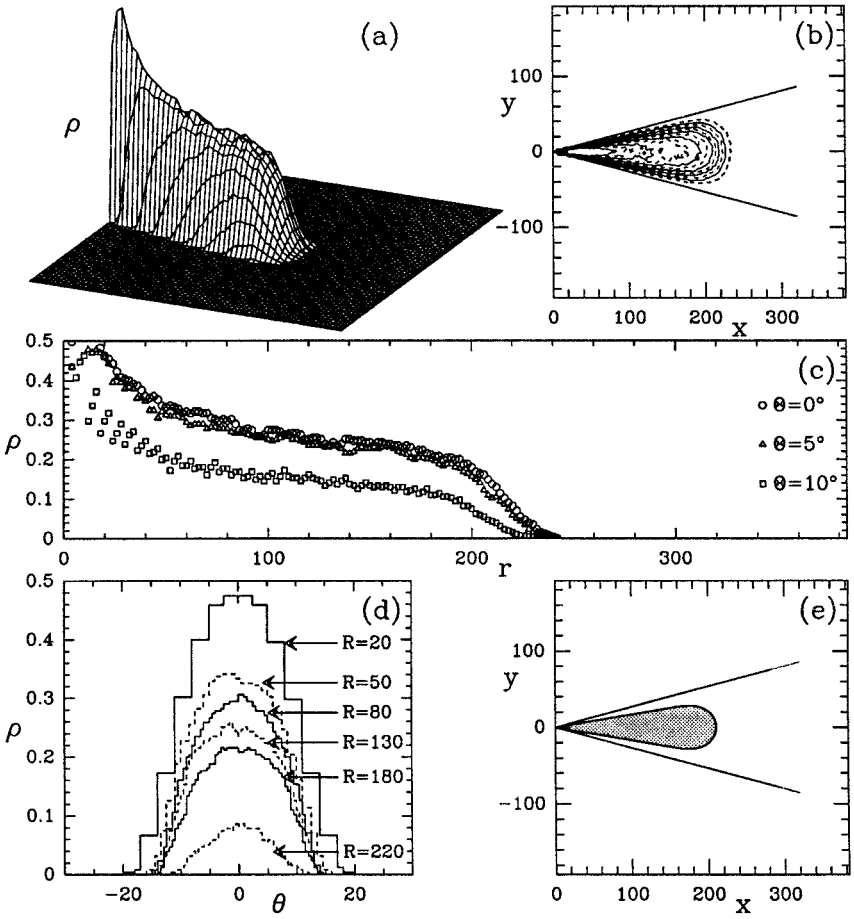

FIG. 17. Statistical analysis of off-lattice DLA clusters of mass $M=2000$ grown in a wedge of angle $\theta_0=30°$. Our statistical sample involves $N=2000$ aggregates similar to the one shown in Fig. 16(a). (a) Three-dimensional representation of the mean occupancy $\rho(r,\theta)$. (b) Contour plots for ρ; the levels correspond to $0.025n$ for $n=1-10$ from outer to inner. (c) Histogram of mean radial occupancy $\rho(r,\theta=\Theta)$ for $\Theta=0°$, 5°, 10°. (d) Histogram of mean azimuthal occupancy $\rho(r=R,\theta)$ for different radii R. (e) In gray is represented the region of large occupancy as defined in Eqs (24) and (25) (see text); in the active front zone the selected points satisfy $\rho(r,\theta)\geqslant\rho(R_{\max},\theta^{\pm}(R_{\max}))$, where $R_{\max}=180$ delimits the frozen region where the growth has ceased. The solid line corresponds to Ben Amar's analytical solution of relative width $\lambda=0.65$.

Whatever the criterion one uses, the relative angular width λ is found larger than $\frac{1}{2}$. When using Eq. (25), one gets a value $\lambda=0.65\pm0.02$ for off-lattice DLA clusters, which is again significantly larger than the estimate $\lambda=0.58\pm0.03$ obtained for a similar statistical sample of $N=2000$ on-lattice DLA clusters of the same mass [29,57]. But what is still very impressive is the agreement observed in Fig. 17(e) between the region of large occupancy defined by selecting the points of the sector cell such that $\rho(r,\theta)\geqslant\rho(r,\theta^{\pm}(r))$ and the self-dilating finger shape of the same relative angular width λ calculated analytically by Ben Amar [46] in the absence of surface tension. Let us further point out that the numerical value $\lambda\sim0.65$ is quite compatible with the relative width predicted for stable fingers belonging to the branch $\lambda_{n=0}(\theta_0=30°,B)$ selected by surface tension [46], provided one identifies the capillary length l_c to a few particle sizes as previously pointed out in linear geometry. It is not such a surprise that the cell geometry should determine the large-scale shape of the profile of mean occupancy. It is a very striking result, however, that the selected solution should be reminiscent of the stable one. In sector-shaped cells, when the structure diverges from the apex, a fractal structure builds up in a larger and larger range of scales between l_c and $r\theta_0$. During this buildup it seems to retain the same sensitivity to both the large and the small scales. In other words, the selection action of the microscopic length scale is likely to act through the entire range, up to the largest scale of the pattern.

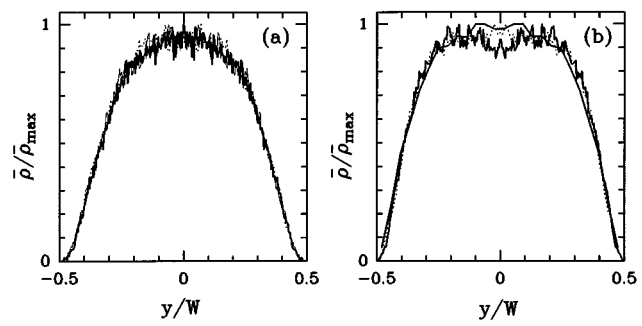

FIG. 18. Rescaled mean azimuthal occupancy histogram $\rho(r=R,\theta)/\rho(r=R,\theta=0)$ for various radii. (a) $\theta_0=30°$: $R=400$ (—), 500 (---), and 700 (—). (b) $\theta_0=60°$: $R=25$ (—), 125 (---), and 225 (—). In both (a) and (b), our statistical sample involves $N=2000$ off-lattice DLA clusters of mass $M=2000$ and 12 000, respectively.

When opening the wedge angle θ_0, one observes some drastic change in the shape of the mean occupancy distribution as shown in Figs. 19 and 20 for $\theta_0=90°$ ($N=2000$, $M=3000$) and 120° ($N=2000$, $M=12\,000$), respectively. When increasing θ_0, the mean profile becomes flatter in the center of the cell with a steeper decrease to zero on both sides of this central plateau. This evolution is clearly illustrated in Fig. 19(d) where the mean azimuthal occupancy histograms computed at different radii for $\theta_0=90°$ all display a very pronounced steplike profile. Simultaneously, the contour plots in Fig. 19(b) become flatter in their most advanced part away from the apex. Moreover, as shown in Fig. 20, if one keeps increasing θ_0, a topological change is observed on

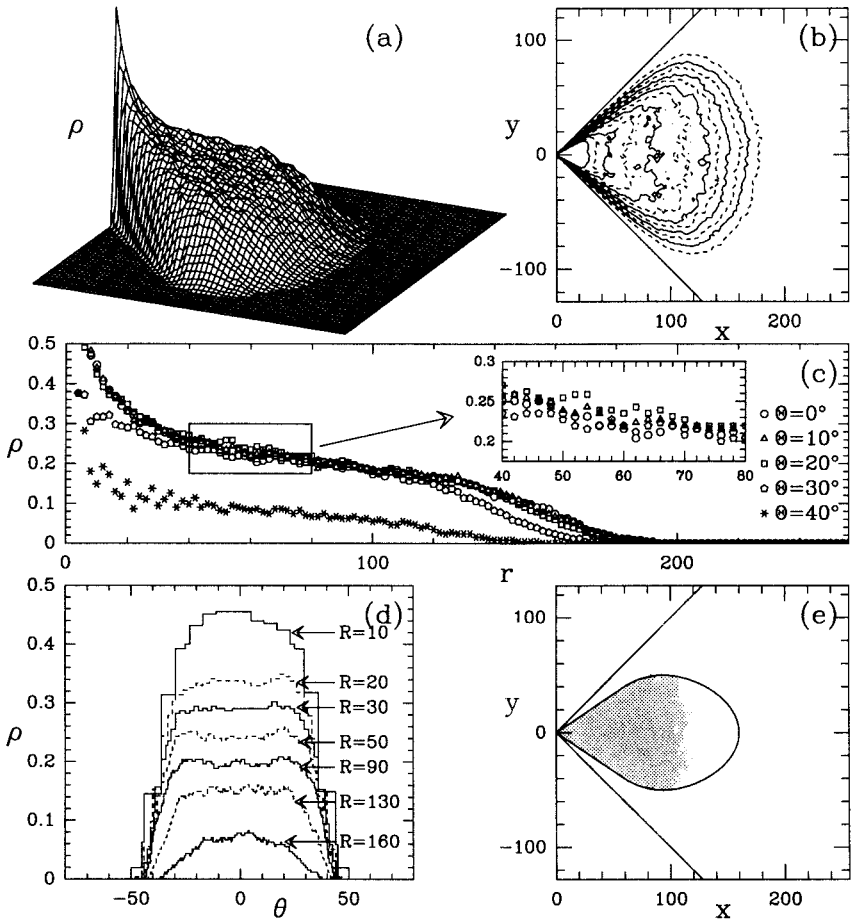

FIG. 19. Statistical analysis of $N=2000$ off-lattice DLA clusters of mass $M=3000$ grown in a wedge of angle $\theta_0=90°$. Same representations as in Fig. 17. In (e) the contour plot $\rho=0.176$ that delimits the shaded region is compared to Ben Amar's analytical solution of relative angular width $\lambda=0.77$ (solid line).

the mean occupancy distribution. Two lobes emerge on both sides of this distribution, one symmetric with the other with respect to the bisector as a result of the averaging procedure over many DLA realizations (let us note that the appearance of these two lobes could have already been guessed from a careful examination of Fig. 19 for $\theta_0=90°$, where this phenomenon is on the verge of emerging). Then, as shown in Figs. 19(c) and 20(c), the mean radial occupancy histograms $\rho(r)=\rho(r,\theta=\Theta)$ computed for different values of Θ cross through each other near the center of the sector; this phenomenon has been called ''profile crossing'' in Ref. [61]. Unlike the channel case, the mean azimuthal histograms $\rho(r=R,\theta)$ computed for various radii R in Fig. 20(d) have a bimodal profile with two maxima that have emerged on the edges of the plateau and a minimum at the center $\theta=0$. This is a clear indication that the growth probability is no longer maximum along the bisector. Although the stiffness of the mean azimuthal profile allows us to define a mean relative angular width λ occupied by our ensemble-averaged DLA patterns, the fact that these profiles are no longer unimodal makes rather questionable the definition of a mean finger shape to be compared with the analytical solutions of Ben Amar [46]. Indeed, as seen in Fig. 20(b), while the different contour plots have almost the same relative angular width $\lambda\sim0.77\pm0.03$, they have drastically different shapes. The lowest level curves corresponding to small occupancy ($\rho\leqslant0.1$) have the shape of a single finger, but they differ from Ben Amar's analytical solutions since they are much flatter in the front zone [112] [see the direct comparison in Fig. 19(e) for $\theta_0=90°$]. The highest level curves of large occupancy have a different shape, which qualitatively resembles a viscous finger pattern after tip splitting [21,28] [Fig. 20(e)]. Thus the comparison of these contour plots with Ben Amar's self-dilating finger solutions is no longer pertinent.

In fact, if, for a given value of the wedge angle θ_0, one averages (unlike in Fig. 17) over DLA clusters of larger and larger mass, ultimately one will reach a value of M for which the mean-occupancy distribution will display the transition from a unimodal to a bimodal profile in the frozen region behind the active front zone. Then, as shown in Fig. 18(b) for $\theta_0=60°$, the mean azimuthal occupancy histograms computed at different radii R can no longer be rescaled onto a unique profile. This indicates that for a given wedge angle θ_0 and a given mass M large enough, the shape of the mean occupancy distribution constantly evolves from a unimodal towards a bimodal profile. Therefore the search of a mean single finger shape underlying the unstable DLA growth in a wedge is no longer justified. Actually, the mean occupancy distribution is likely to retain some memory of the whole set of stable fingers that belong to the branch $\lambda_{n=0}(\theta,B)$ selected by surface tension up to the critical value B_c where this branch collides with the unstable branch $\lambda_{n=1}(\theta,B)$ and disappears [46–49]. Once the size of the finger goes beyond this merging threshold, tip splitting occurs and there is no stable smooth finger in the sector geometry for small B (i.e., large $W=r\theta_0$). The topological change from a unimodal to a bimodal profile of the mean occupancy distribution can thus be seen as the footprint of the tip-splitting instability of vis-

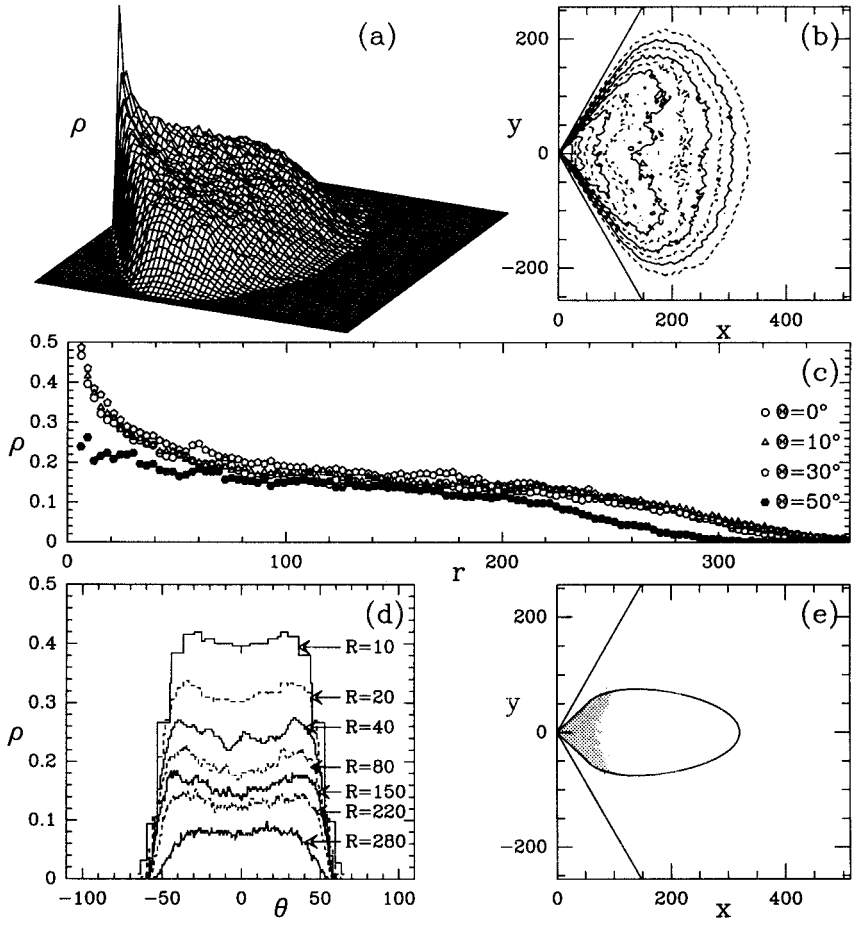

FIG. 20. Statistical analysis of $N=2000$ off-lattice DLA clusters of mass $M=12\,000$ grown in a wedge of angle $\theta_0=120°$. Same representations as in Fig. 17. In (e) the contour plot $\rho=0.196$ that delimits the shaded region is compared to Ben Amar's analytical solution of relative angular width $\lambda=0.77$ (solid line).

cous fingers growing in a wedge. Since this branch merging is induced by surface tension, its indirect observation on the ensemble-averaged DLA patterns confirms the selective role of the microscopic length scale, i.e., the particle size, in DLA growth.

From a statistical point of view, one can try to interpret the global shape of the mean occupancy distribution as the superposition of many realizations, some of which correspond to a single main fractal branch that is well developed in the central part of the wedge, while some others are mainly made of two main branches that have grown on either side of the bisector. The latter realizations being obviously shorter since the total mass is shared by two branches could explain the presence of the two lobes in the inner frozen region of $\rho(r,\theta)$ [Fig. 20(a)]. In the active front zone, the mean azimuthal histogram recovers a unimodal profile [Figs. 19(d) and 20(d)] since most of the realizations that contribute so far away from the apex consist in DLA clusters that have not produced secondary fractal branches. Actually, as discovered in Refs. [74,75,113,114], the inner frozen region of DLA clusters is likely to display a statistically predominant Fibonacci structural ordering. One can therefore expect to observe some further topological changes (some further branchings in the contour plots) in the mean occupancy profile when further increasing the mass M. However, some specific treatment on each realization is required in order to prevent the averaging procedure to restore the symmetry with respect to the bisector. This work is currently in progress.

For the sake of comparison, we have reproduced our statistical analysis of DLA clusters in a wedge using an on-lattice algorithm [57], the bisector being one of the axes of the underlying square lattice. For small sector angles and small mass clusters, the mean occupancy distribution does not seem to be very much affected by the lattice anisotropy. This is no longer the case if one increases the mass M. As shown in Fig. 21, for a wedge angle $\theta_0=120°$, the presence of the underlying lattice favors the growth along the lattice axis, thereby inhibiting the transition to a bimodal mean occupancy distribution [61]. The mean radial histograms no longer display the ''profile crossing'' phenomenon observed for off-lattice DLA simulations [Fig. 21(c)]. The mean azimuthal histograms have again a unique maximum at the center $\theta=0$ [Fig. 21(d)]. The contour plots in Fig. 21(b) have a squarelike shape similar to the petal shape of anomalous viscous fingers in the presence of fourfold anisotropy [115,116]. When proceeding to large-mass simulations, one can check that the mean relative width λ of these ensemble-averaged DLA patterns, calculated using Eq. (24) with either Eq. (25) or Eq. (26) to define $\theta^{\pm}(r)$, systematically decreases towards zero when going away from the apex. This anisotropy-induced stabilization of the ''normal'' unimodal pattern with maximum density always along the bisector regardless of the distance of the apex is again very reminiscent of what is theoretically predicted and experimentally observed for stable viscous patterns. Ben Amar has shown in Ref. [115] that adding a sufficient anisotropy can eliminate the branch merging phenomenon and allow the stable finger solution

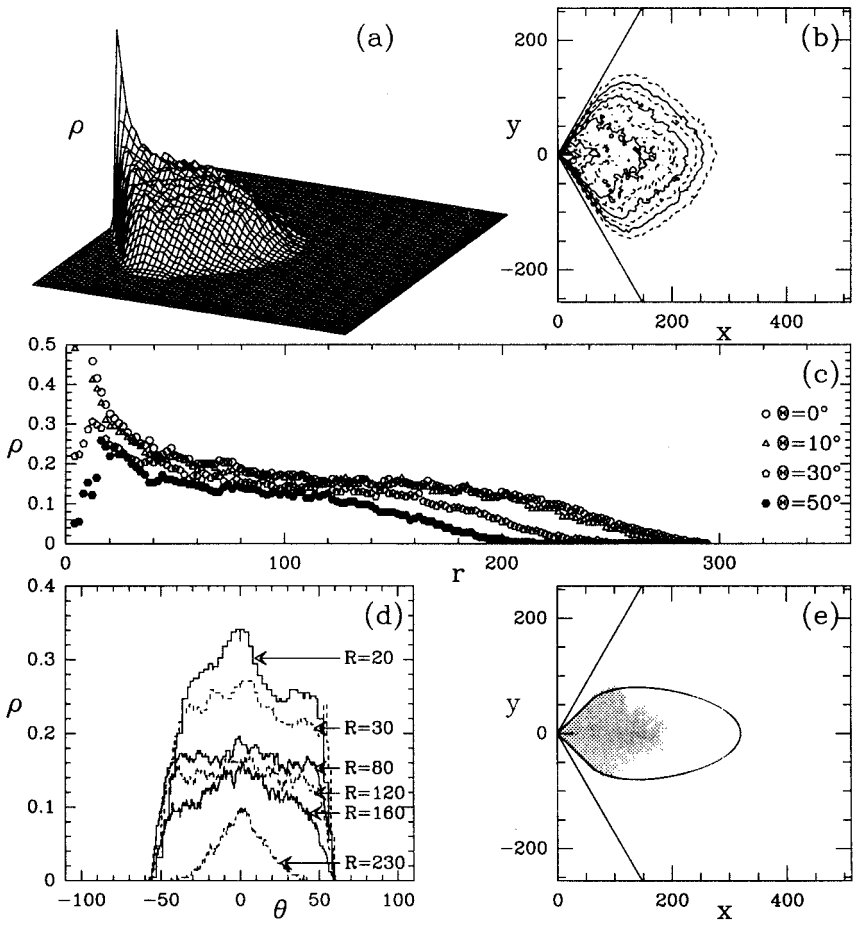

FIG. 21. Statistical analysis of $N=1000$ on-lattice DLA clusters of mass $M=6000$ grown in a wedge of angle $\theta_0=120°$. (a) Three-dimensional representation of the mean occupancy $\rho(r,\theta)$. (b) Contour plots for ρ; the levels correspond to $0.025n$ for $n=1-10$ from outer to inner. (c) Histogram of mean radial occupancy $\rho(r=R,\ \theta=\Theta)$ for different values of Θ. (d) Histogram of mean azimuthal occupancy $\rho(r=R,\theta)$ for different radii R. (e) The contour plot $\rho=0.137$ that delimits the shaded region is compared to Ben Amar's analytical solution of relative angular width $\lambda=0.75$ (solid line).

branch $\lambda_{n=0}(\theta_0,B)$ to survive in the limit $B\to 0$ (i.e., $W=r\theta_0\to+\infty$). Actually $\lambda_{n=0}(\theta_0,B)$ is predicted to converge to zero in this asymptotic limit. Anomalous viscous fingers growing in a wedge are therefore stabilized with respect to tip splitting by anisotropy. We are claiming only that the ensemble-averaged on-lattice DLA structures are also sensitive to these considerations.

B. Mean-field diffusion-limited aggregation

The generalization of the mean-field approach described in Sec. II B from channel to radial geometries was first performed by Levine and Tu in Ref. [61]. For sectors, the mean-field equation (9) takes the following form when using polar coordinates:

$$\frac{\partial\rho}{\partial t}=\left(\frac{1}{r^2}\frac{\partial^2}{\partial\theta^2}+\frac{\partial^2}{\partial r^2}+\frac{1}{r}\frac{\partial}{\partial r}\right)u, \tag{27a}$$

$$\frac{\partial\rho}{\partial t}=u\left[\rho^{\gamma}+a^2\left(\frac{1}{r^2}\frac{\partial^2}{\partial\theta^2}+\frac{\partial^2}{\partial r^2}+\frac{1}{r}\frac{\partial}{\partial r}\right)\rho\right]. \tag{27b}$$

Again, we impose Neuman boundary conditions for the u field:

$$\vec{n}\cdot\nabla u|_{\theta=\pm\theta_0/2}=0, \tag{28}$$

where $\vec{n}$ is the normal to the side walls and Dirichlet condition for the ρ field:

$$\rho|_{\theta=\pm\theta_0/2}=0. \tag{29}$$

As $r\to+\infty$, we impose that $\partial u/\partial r=c/r$, where c is the rate at which particles are being released. Practically, we fix the flux of the ''walkers'' at the far end extremity of the wedge:

$$\left.\frac{\partial u}{\partial r}\right|_{r=L}=\frac{\varphi}{L}. \tag{30}$$

As in linear geometry, from some adequate rescalings of t, r, and the fields ρ and u, one can fix the lattice spacing and the flux to unity: $a=\varphi=1$.

In this section, we report the results of the numerical integration of Eq. (27) with the boundary conditions (28), (29), and (30) for various values of γ and θ_0, which are the only free parameters left to this mean-field approach. The resolution used to compute the ρ and u fields is similar to those previously considered for linear strips: in polar coordinates (r,θ), we use lattices of size $L\times 40$, where $L\in[50,200]$ is adjusted according to the final size of the mean growth one intends to achieve. Also, we explicitly impose symmetry about the bisector by starting from an initial condition for the ρ field that is invariant under this symmetry. The numerical procedure is again based on the fact that u is a ''passive'' field without any proper dynamics. At a fixed time, we can thus find u directly from the ρ field; we then update ρ and continue.

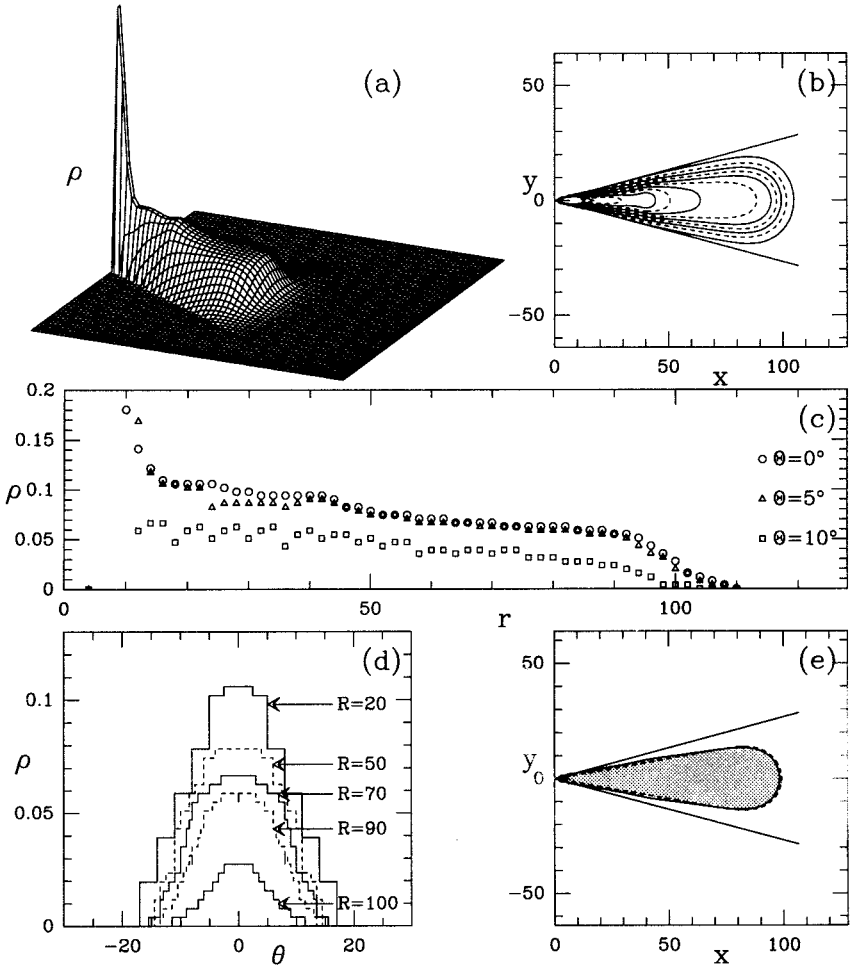

FIG. 22. Mean-field calculation of the ρ field distribution in a wedge of angle $\theta_0=30°$; the model parameters are $\varphi=1$, $\gamma=2$, $a=1$. (a) Three-dimensional representation of $\rho(r,\theta)$. (b) Contour plots for ρ; the levels are $0.01n$ for $n=1-10$ from outer to inner. (c) Radial density profiles: $\rho(r,\theta=\Theta)$ for $\Theta=0°$, 5°, and 10°. (d) Azimuthal density profiles: $\rho(r=R,\theta)$ for different radii R. (e) In gray is represented the region of large DLA occupancy [Fig. 17(e)]; the solid line corresponds to the mean-field calculation of the boundary of this region; Ben Amar's analytical finger of width $\lambda=0.65$ is represented by the dashed line.

In Figs. 22 and 23 are reported the numerical ρ profiles computed with the mean field equation (27) for two wedges of respective angle $\theta_0=30°$ and 120°. The value of the cutoff parameter is $\gamma=2$ as in Ref. [61]. In the small-angle wedge (Fig. 22), after some transients, the aggregate field ρ starts developing with a rather compact fingerlike profile that is very similar to the shape of the mean occupancy distribution of off-lattice DLA clusters in the early stage of growth (Fig. 17). As seen on both the radial profiles [Fig. 22(c)] and the azimuthal profiles [Fig. 22(d)], the ρ density is maximum along the bisector. The former decreases smoothly when one moves radially away from the apex until one reaches the exponential falloff in the active front zone. The latters display a unimodal characteristic shape centered at $\theta=0$. As shown in Fig. 24(a), these azimuthal ρ profiles computed at different radii in the frozen region are nearly self-similar since they can be almost rescaled onto a unique profile. Therefore, one can reasonably use either the criteria (25) or (26) to define a mean relative angular width λ [Eq. (24)] of the ρ density. When using Eq. (25), one gets the value $\lambda=0.67\pm0.01$, which is in remarkable quantitative agreement with the estimate obtained for ensemble-averaged off-lattice DLA patterns in Fig. 17. In Fig. 22(e), the region of large ρ density (solid line) as defined by selecting the points of the sector cell such that $\rho(r,\theta)\geqslant\rho(r,\theta^{\pm}(r))$ is compared to Ben Amar's analytic finger solution (dashed line) of equal relative angular width in the absence of surface tension [46]; the two profiles are indistinguishable. Moreover, they provide a very good fit of the boundary of the large occupancy region of off-lattice DLA clusters (shaded area); let us note that this self-similar region has been rescaled from Fig. 17(e) to Fig. 22(e) in order to position its tip at the same location as the tip of the mean mean-field finger. More generally, the contour plots of the ρ density in Fig. 22(b) are quite comparable to the finger-shaped level curves of the ensemble-averaged DLA pattern in Fig. 17(b).

If one proceeds to more time consuming simulations of the mean-field equation, one realizes very quickly that the self-similar regime observed in the early stage of growth is nothing more than a transient phenomenon. Indeed, the profile of the ρ field in the frozen region constantly evolves from a unimodal to a bimodal profile. This is illustrated in Fig. 24(b) where the azimuthal ρ profile calculated in a cell of angle $\theta_0=60°$ becomes flatter and flatter at the top when one moves further away from the apex, until one goes beyond some critical radius where two shoulders appear on the edges of this steplike profile. This topological transition is strikingly similar to the one observed in ensemble-averaged DLA patterns in Fig. 18(b). The larger the angle of the cell, the smaller the critical radius, i.e., the sooner the morphological transition from a unimodal to a bimodal ρ profile takes place. When comparing the results of the mean-field calculations for $\theta_0=120°$ in Fig. 23 to the corresponding mean occupancy DLA distribution in Fig. 20, one observes similar features

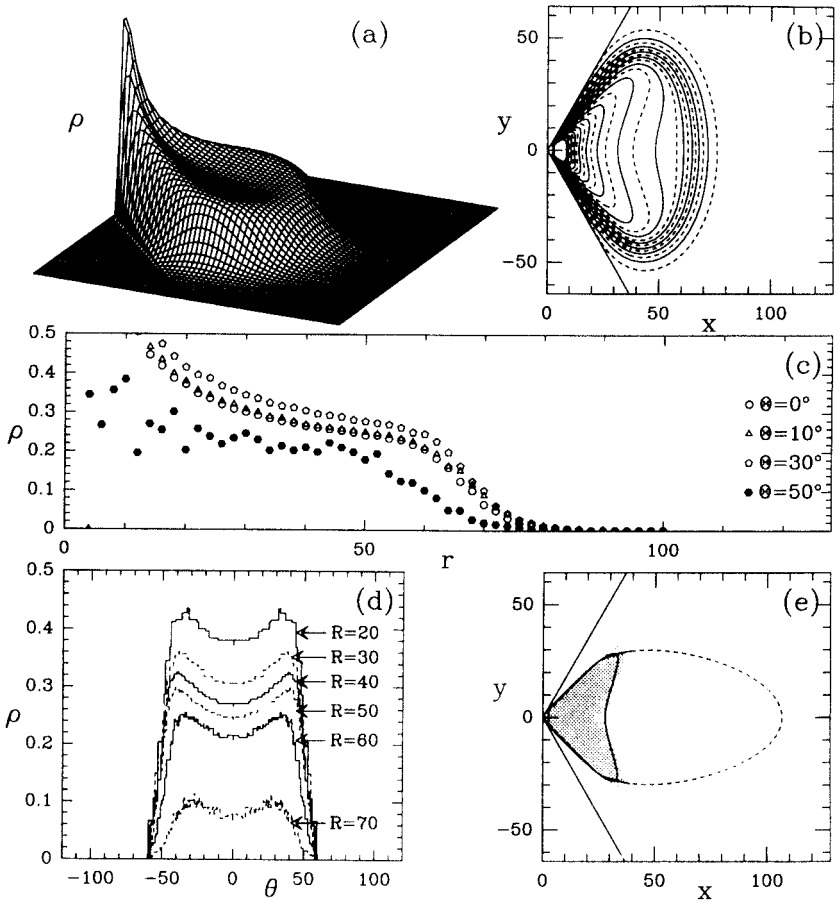

FIG. 23. Mean-field calculation of the ρ field distribution in a wedge of angle $\theta_0=120°$. Same representations and same model parameters as in Fig. 22.

that are characteristic of this morphological transition. The radial ρ profile in Fig. 23(c) presents the profile crossing phenomenon detected in Fig. 20(c). The azimuthal ρ profiles in Fig. 23(d) are no longer maximum but are minimum at the center; they display two maxima symmetric with each other with respect to the center as observed in Fig. 20(d). The contour plots in Fig. 23(b) have drastically different shapes as in Fig. 20(b): the lowest level curves of small ρ density have the shape of very flat fingers, while the highest level curves of large ρ density have a tip-splitted finger shape. As shown in Fig. 23(e), these highest level curves are quite comparable with the highest contour plots of the mean occupancy of off-lattice DLA clusters and obviously clearly differ from Ben Amar's analytical solutions. Indeed none of the ρ contour plots corresponds to a member of Ben Amar's solution family [46]. This is not suprising since, as previously discussed, there is no stable smooth finger in the sector geometry for small B, i.e., in the limit of large size, because of intrinsic tip-splitting instability [20,46]. The results reported in this section show that in this unstable regime, while the comparison of the ensemble-averaged DLA patterns with ST finger profiles no longer works, the mean-field theory still accounts, at least at a qualitative level, for the topological characteristics of the mean occupancy distribution computed in off-lattice DLA simulations.

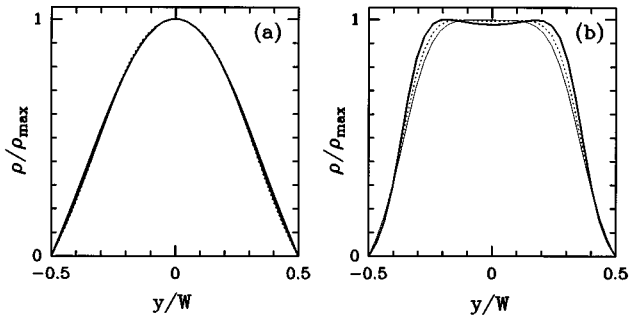

FIG. 24. Rescaled azimuthal density profiles: $\rho(r=R,\theta)/\rho(r=R,\theta=0)$ for various radii. (a) $\theta_0=30°$: $R=30$ (—), 50 (---), and 70 (—). (b) $\theta_0=60°$: $R=20$ (—), 60 (---), and 80 (—).

C. Fractal analysis

If off-lattice DLA clusters grown in sector geometries are homogeneous fractal aggregates as seems to be the case in circular geometry [74,75,108–110], the exponent of the singularity located at the apex of the wedge is identical to the singularity exponent at any other cluster point. In other words, the way the mass contained in a ball scales as a function of the size of the ball does not depend upon the point where the ball is centered, provided this point belongs to the cluster: $M(\mathscr{B}(\vec{x},\epsilon))\propto\epsilon^{D_F}$, where D_F is the fractal dimension of the DLA cluster. A way of computing D_F therefore consists in integrating the mean occupancy distribution over all of the sector up to some radius R:

$$M(R)=\int_0^R\int_{-\theta_0/2}^{\theta_0/2}\rho(r,\theta)r\,dr\,d\theta\propto R^{D_F}. \tag{31}$$

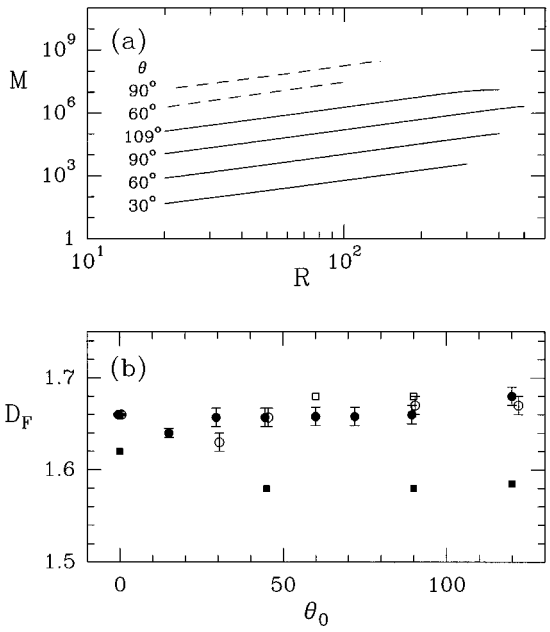

FIG. 25. Estimate of the fractal dimension D_F from the radial dependence of the mass according to Eq. (31). (a) $\log M$ vs $\log R$: (—) off-lattice simulations; (---) mean-field calculations. (b) D_F vs θ_0. The symbols have the following meaning: ●, off-lattice DLA simulations; ○, on-lattice DLA simulations; ■, mean-field calculations with $\gamma=2$; □, mean-field calculations with $\gamma=1.6$.

In Fig. 25 are reported the estimates of D_F from large-mass off-lattice DLA simulations in sectors of angle ranging from 15° to 120°. As seen in Fig. 25(a), when plotting $M(R)$ defined in Eq. (31) versus R in a log-log representation, one observes a very nice scaling behavior in an intermediate range of values of R, which corresponds to the frozen region left behind the active outer front zone. From a linear regression fit of these numerical data, one extracts the values of the fractal dimension D_F, which does not seem to depend upon the value of the wedge angle θ_0. Indeed, the data in Fig. 25(b) are quite compatible with the estimate $D_F=1.66\pm0.01$ previously obtained in strip geometry (Fig. 13), i.e., for $\theta_0=0$. Let us point out that on-lattice DLA simulations yield a similar θ_0-independent estimate of D_F, which, up to the numerical uncertainty, cannot be distinguished from the off-lattice value $\frac{5}{3}$. We recall that this numerical estimate is in perfect agreement with the theoretical prediction $D_F=(d^2+1)/(d+1)$ for diffusion-limited aggregation in d dimensions [103–105].

Figure 25 also shows for comparison the estimates of the fractal dimension D_F from the mean-field calculations described in Sec. III B. Again D_F does not show any significant dependence upon the wedge angle θ_0. For $\gamma=2$, we therefore recover a value of D_F that as in linear geometry ($D_F=1.58\pm0.01$), slightly underestimates the value extracted from ensemble-averaged DLA patterns. For other values of the cutoff parameter γ, one gets estimates that are all in good agreement with the results obtained in channel geometry (Fig. 14). As discussed in Sec. II C, the mean-field theory formulated in Eq. (27) is likely to predict a fractal dimension that matches the DLA value $D_F=\frac{5}{3}$ for only two values of γ, namely, $\gamma\sim1.6$ and 4.2. The estimates of D_F for $\gamma=1.6$, in wedges of various angles θ_0, are shown in Fig. 25; they actually lie in the error bars of both on-lattice and off-lattice data.

But very much like what we have already noticed in linear geometry (see Fig. 15), the fact that for $\gamma=1.6$ and 4.2 the mean-field theory accounts for the radial dependence of the mass does not mean that it quantitatively reproduces the radial evolution of the shape of the mean occupancy profile. We have checked that this is indeed not the case. For wedges of arbitrary angle θ_0, the comparison of the shapes of the mean-field azimuthal ρ profile at different radial positions with the corresponding mean azimuthal DLA occupancy histograms reveals some quantitative discrepancies, although they both exhibit a transition from a unimodal to a bimodal profile. Actually, for DLA clusters of a given mass M grown in a wedge of angle θ_0, there is no time at which one can stop the mean-field calculation so that after some radial rescaling in order to adjust the position of the active front zone, the ρ contour lines match exactly the level curves of the mean DLA occupancy distribution. This is the confirmation that, as formulated in Eq. (27), the mean-field approach provides a good approximation of the ensemble-averaged DLA structures in sector geometry, but fails to pass any quantitative comparison test. In that sense, this generalization of Witten and Sander's original mean-field approach still deserves some additional refinements.

IV. DISCUSSION

To summarize briefly, we have carried out a statistical analysis of off-lattice DLA clusters grown in either linear or sector geometry. We have compared the mean occupancy distributions to the predictions of a recently adapted version [60,61] of the mean-field approach originally proposed by Witten and Sander [50]. In channels, the walls impose translational invariance to the mean occupancy, which is found to converge to a smooth asymptotic profile when increasing the width W of the strip. The shape of this profile is likely to be selected by surface tension, the size of the aggregating particles playing the role of the capillary length in viscous fingering. Actually, we have shown that the region of large occupancy, as defined by some contour plot [Eq. (6)], has exactly the shape of a Saffman-Taylor finger with a relative with $\lambda(W)$ that converges to $\frac{1}{2}$ when increasing W, as expected from the theory of stable fingers [34–40]. This indicates that the off-lattice algorithm has removed the crossover phenomenon from isotropic to dendritic fractal DLA patterns observed in on-lattice simulations [58,59] with a mean relative width $\lambda(W)$ that converges ultimately to zero in the limit $W\rightarrow+\infty$. In sector geometry, the comparison of the DLA mean occupancy profile to ST fingers is no longer relevant since, as shown in Refs. [46–49], the presence of finite surface tension prevents the stable finger from reaching an asymptotic self-similar shape of finite relative angular width. At a critical size that depends upon the cell angle θ_0, this finger becomes unstable due to the so-called tip-splitting instability. What our off-lattice DLA simulations in sector geometry show is that, except in the early stage of growth in small-angle cells where some connection to stable ST fingers can still be achieved, the mean occupancy distribution is not self-similar in the sense that it cannot be radially rescaled

onto a unique asymptotic profile. Actually, the shape of the ensemble-averaged DLA pattern constantly evolves from a unimodal profile close to the apex towards a bimodal profile beyond some critical radius. This topological change of the DLA mean occupancy profile is strikingly reminiscent of the morphological tip-splitting instability of ST fingers. This is again a strong indication that surface tension is present in DLA growth and that the microscopic scale introduced by the size of the aggregating particles actually governs the selection of a particular mean-occupancy profile. Let us emphasize that this topological transition in the mean-occupancy distribution was not observed in previous studies of on-lattice DLA clusters [57]. Very much like the anisotropy-induced stabilization of anomalous ST fingers [115], the lattice anisotropy stabilizes the unimodal finger-shaped mean occupancy profile, which no longer bifurcates into a bimodal profile but progressively crosses over to a petal finger shape with a relative radial width that asymptotically converges to zero.

When solving numerically the mean-field equations [60,61], for almost any arbitrary values of the cutoff parameter γ, one gets solutions that qualitatively mimic most of the characteristic features displayed by the ensemble-averaged DLA patterns in linear as well as in sector geometries. As shown by Levine and Tu [61], one can even model the results of the on-lattice DLA simulations by including some anisotropy in the mean-field equations. However, there is a gap between qualitative and quantitative modeling. In particular, when computing the fractal dimension D_F of DLA clusters from the scaling properties of the integrated (over spatial coordinates) aggregate ρ field, we have found that most of the values of the cutoff parameter γ do not yield the dimension $D_F=\frac{5}{3}$ extracted from both off-lattice and on-lattice simulations. Actually, only two values of γ, namely, $\gamma\sim 1.6$ and 4.2, seem to give satisfactory estimates. Unfortunately, for each of these two values, the mean-field ρ profiles computed in both linear and sector geometries cannot be quantitatively rescaled onto the corresponding numerical DLA mean-occupancy profiles. This discrepancy indicates that the revised mean-field approach prompted by Brener, Levine, and Tu [60] in linear geometry and Levine and Tu [61] in sector geometry is still a premature theory that certainly deserves further improvement.

A rather naive idea would consist in introducing some higher order terms in the ρ field variable in both Eqs. (9b) and (27b). As shown in Fig. 26(a), when choosing $\gamma=1.6$ and adding a quadratic term $c\rho^2$ in Eq. (9b), one can find a value of c such that the transverse ρ profile coincides with the mean transverse occupancy profile of DLA growth in a channel of width $W=64$. Unfortunately this same value of c does not work for wider channels as seen in Fig. 26(b) for $W=128$. Nevertheless, one can still hope to remedy this discrepancy by considering additional higher order terms in order to have more free parameters at our disposal. However, one can show that this strategy is hopeless. Let us rewrite Eq. (9b) under a more general form:

$$\partial\rho/\partial t = u[(f(\rho)+a^2\nabla^2\rho)], \tag{32}$$

where f is an unknown function of ρ. Some insight to the specific shape of this function can be gained from our off-lattice DLA simulations by noticing that the mean transverse occupancy profile satisfies the steady-state equation:

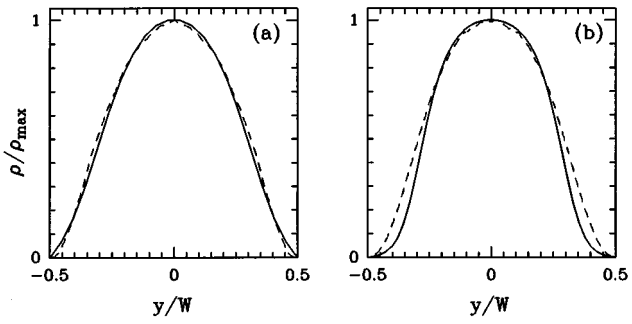

FIG. 26. Same as in Fig. 15 except that some quadratic term $c\rho^2$ has been added to the ρ^γ term in the right-hand side of mean-field equation (9b).

$$f(\rho_T) = -a^2\partial^2\rho_T/\partial y^2. \tag{33}$$

The validity of Eq. (33) relies on the fact that the overall mean-occupancy profile displays translational invariance in the frozen region behind the active front zone. From the fractal analysis carried out in Sec. II C, we know that this transverse profile scales as

$$\rho_T(y) = W^{D_F-2}\mathscr{R}(y/W), \tag{34}$$

when considering channels of different widths. Here $\mathscr{R}(x)$ is a universal, W independent, profile. From Eqs. (33) and (34), we have represented in Fig. 27, $-W^{4-D_F}\partial^2\rho_T/\partial y^2$ as a function of $W^{2-D_F}\rho_T$. The data obtained from the DLA mean transverse profiles computed at different channel widths $W=48$, 80, 96, and 112, all fall on a similar curve (let us note that the oscillations observed for large values of ρ_T are the consequence of statistical fluctuations in the estimate of ρ_T in the central part of the channel where ρ_T is maximum). This observation brings the clue that $f(\rho)$ is likely to be a smooth nonlinear function of ρ that definitely depends upon the width W of the channel. This is experimental evidence that explains *a posteriori* why the revised mean-field

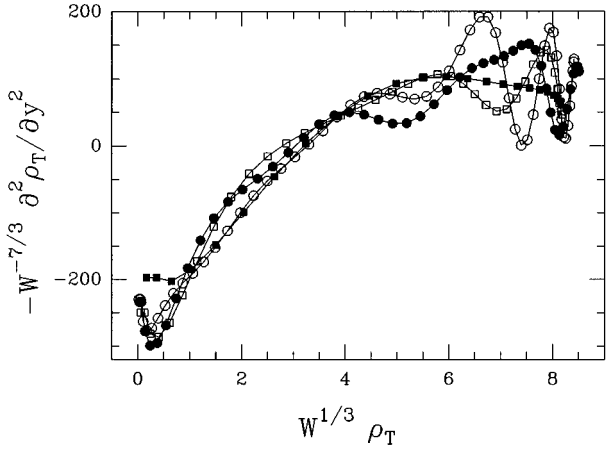

FIG. 27. $-W^{7/3}\partial^2\rho_T/\partial y^2$ vs $W^{1/3}\rho_T$ where ρ_T is the mean transverse occupancy profile extracted from off-lattice DLA simulations in linear strips of width $W=48$ (■), 80 (□), 96 (●), and 112 (○).

theory fails to account for the width dependence of the ensemble-averaged DLA patterns. Moreover, the results in Fig. 27 show that $f(\rho)$ becomes negative for values $\rho<\rho_c$, where ρ_c is some finite value, contrarly to all the modelings proposed so far, e.g., $f(\rho)=\rho^\gamma$ or $\rho\Theta(\rho-c)$ [60] (where Θ is the Heaviside function). The DLA data therefore do not accommodate of a mean-field model with a single nonlinear term $f(\rho)=\rho^\gamma$.

To understand the inadequacy of the mean-field theory proposed by Brener, Levine, and Tu [60] and Levine and Tu [61], one has to come back to the original work of Witten and Sander [50]. It is clear that one of the main ingredients of this approach and probably one of its main weaknesses is the fact that the aggregate is considered to be transparent to the diffusing particles [100]. This is undoubtedly a very questionable working hypothesis. It is probable that a more realistic mean-field theory would consist in making the aggregate opaque to the diffusion field. Actually, the fact that $f(\rho)<0$ if $\rho<\rho_c$ (Fig. 27) can be interpreted as introducing an additional cutoff to the growth rate term ρ^γ, which is probably due to the nonpenetrability of the aggregate to the random walkers. There has been some recent attempts to elaborate in this direction in Ref. [117]. As represented in Fig. 27, the results of our statistical analysis of off-lattice DLA clusters are likely to provide a decisive test for future mean-field approaches of diffusion-limited aggregation.

ACKNOWLEDGMENTS

We are very grateful to F. Argoul, M. Ben Amar, Y. Couder, and J. F. Muzy for very helpful discussions. We acknowledge computing resources from IDRIS (Project No. 940087) and pole MNI (University of Bordeaux I).

[1] J. S. Langer, Rev. Mod. Phys. **52**, 1 (1980).
[2] S. C. Huang and M. E. Glicksman, Acta Metall. **29**, 701 (1981).
[3] D. Bensimon, L. P. Kadanoff, S. Liang, B. I. Shraiman, and C. Tang, Rev. Mod. Phys. **58**, 977 (1986).
[4] J. S. Langer, in *Chance and Matter*, edited by J. Souletie, J. Vanimenus, and R. Stora (North-Holland, Amsterdam, 1987).
[5] D. A. Kessler, J. Koplik, and H. Levine, Adv. Phys. **37**, 255 (1988).
[6] P. Pelcé, *Dynamics of Curved Fronts* (Academic, Orlando, 1988).
[7] J. S. Langer, Science **243**, 1150 (1989).
[8] *On Growth and Form: Fractal and Non Fractal Patterns in Physics*, edited by H. E. Stanley and N. Ostrowsky (Martinus Nijhof, Dordrecht, 1986).
[9] *The Physics of Structure Formation*, edited by W. Guttinger and D. Dangelmayr (Springer, Berlin, 1987).
[10] *Random Fluctuations and Pattern Growth*, edited by H. E. Stanley and N. Ostrowsky (Kluwer Academic, Dordrecht, 1988).
[11] J. Feder, *Fractals* (Pergamon, New York, 1988).
[12] T. Vicsek, *Fractal Growth Phenomena* (World Scientific, Singapore, 1989).
[13] *Fractals' Physical Origin and Properties*, edited by L. Pietronero (Plenum, New York, 1989).
[14] C. Evertsz, Ph.D. thesis, University of Groningen, 1989.
[15] *Fractals and Disordered Systems*, edited by A. Bunde and S. Havlin (Springer, Berlin, 1991).
[16] *Growth and Form: Nonlinear Aspects*, edited by M. Ben Amar, P. Pelcé, and P. Tabeling (Plenum, New York, 1991).
[17] *Growth Patterns in Physical Sciences and Biology*, edited by J. M. Garcia-Ruiz, E. Louis, P. Meakin, and L. M. Sander (Plenum, New York, 1993).
[18] *Fractals in Natural Sciences*, edited by T. Vicsek, M. Shlesinger, and M. Matsushita (World Scientific, Singapore, 1994).
[19] P. G. Saffman and G. I. Taylor, Proc. R. Soc. London, Ser. A **245**, 312 (1958).
[20] M. Ben Amar, V. Hakim, M. Mashaal, and Y. Couder, Phys. Fluids A **3**, 1687 (1991).
[21] Y. Couder, in *Chaos, Order and Patterns*, edited by R. Artuso, P. Cvitanovic, and G. Casati (Plenum, New York, 1991), p. 203, and references therein.
[22] L. Paterson, Phys. Rev. Lett. **52**, 1621 (1984).
[23] J. Nittmann, G. Daccord, and H. E. Stanley, Nature **314**, 141 (1985).
[24] Jing-Den Chen and D. Wilkinson, Phys. Rev. Lett. **55**, 1892 (1985).
[25] G. Daccord, J. Nittmann, and H. E. Stanley, Phys. Rev. Lett. **56**, 336 (1986).
[26] S. N. Rauseo, P. D. Barnes, and J. V. Maher, Phys. Rev. A **35**, 1245 (1987).
[27] A. R. Kopf-Sill and G. M. Homsy, Phys. Fluids **31**, 242 (1988).
[28] Y. Couder, in *Random Fluctuations and Pattern Growth* (Ref. [10]), p. 75.
[29] A. Arneodo, F. Argoul, Y. Couder, and M. Rabaud, in *Growth and Form: Nonlinear Aspects* (Ref. [16]), p. 297.
[30] R. L. Chuoke, P. Van Meurs, and C. Van der Pol, Trans. AIME **216**, 188 (1959).
[31] P. Tabeling, G. Zocchi, and A. Libchaber, J. Fluid Mech. **177**, 67 (1987).
[32] J. W. McLean and P. G. Saffman, J. Fluid. Mech. **102**, 445 (1981).
[33] J. M. Vanden-Broeck, Phys. Fluids **26**, 2033 (1983).
[34] R. Combescot, T. Dombre, V. Hakim, Y. Pomeau, and A. Pumir, Phys. Rev. Lett. **56**, 2036 (1986); Phys. Rev. A **37**, 1270 (1988).
[35] B. Shraiman, Phys. Rev. Lett. **56**, 2028 (1986).
[36] D. C. Hong and J. Langer, Phys. Rev. Lett. **56**, 2032 (1986).
[37] D. Bensimon, Phys. Rev. A **33**, 1302 (1986).
[38] D. A. Kessler and H. Levine, Phys. Rev. Lett. **57**, 3069 (1987).
[39] S. Tanveer, Phys. Fluids **30**, 1589 (1987); **30**, 2318 (1987).
[40] D. Bensimon, P. Pelcé, and B. I. Shraiman, J. Phys. (Paris) **48**, 2081 (1987).
[41] H. J. S. Hele-Shaw, Nature **58**, 34 (1898).
[42] H. Thomé, M. Rabaud, V. Hakim, and Y. Couder, Phys. Fluids A **1**, 224 (1989).

[43] J. Bataille, Revue Inst. Pétrole **23**, 1349 (1968).
[44] L. Paterson, J. Fluid Mech. **113**, 513 (1981).
[45] E. A. Brener, D. A. Kessler, H. Levine, and W. J. Rappel, Europhys. Lett. **13**, 161 (1990).
[46] M. Ben Amar, Phys. Rev. A **43**, 5724 (1991); **44**, 3673 (1991).
[47] Y. Tu, Phys. Rev. A **44**, 1203 (1991).
[48] R. Combescot and M. Ben Amar, Phys. Rev. Lett. **67**, 453 (1991).
[49] R. Combescot, Phys. Rev. A **45**, 873 (1992).
[50] T. A. Witten and L. M. Sander, Phys. Rev. Lett. **47**, 1400 (1981); Phys. Rev. B **27**, 5686 (1983).
[51] P. Meakin, in *Phase Transition and Critical Phenomena*, edited by C. Domb and J. L. Lebowitz (Academic, Orlando, 1988), Vol. 12, p. 355.
[52] T. Vicsek, Phys. Rev. Lett. **53**, 2281 (1984); Phys. Rev. A **32**, 3084 (1985).
[53] J. R. Banavar, M. Kohmoto, and J. Roberts, Phys. Rev. A **33**, 2065 (1986).
[54] J. Nittman and H. E. Stanley, J. Phys. A **20**, L1185 (1987).
[55] P. Meakin, F. Family, and T. Vicsek, J. Colloid Interface Sci. **117**, 394 (1987).
[56] R. Tao, M. A. Novotny, and K. Kaski, Phys. Rev. A **38**, 1019 (1988).
[57] A. Arneodo, Y. Couder, G. Grasseau, V. Hakim, and M. Rabaud, Phys. Rev. Lett. **63**, 984 (1989); in *Nonlinear Evolution of Spatio-Temporal Structures in Dissipative Continuous Systems*, edited by F. H. Busse and L. M. Kramer (Plenum, New York, 1990), p. 481.
[58] Y. Couder, F. Argoul, A. Arneodo, J. Maurer, and M. Rabaud, Phys. Rev. A **42**, 3499 (1990).
[59] A. Arneodo, F. Argoul, Y. Couder, and M. Rabaud, Phys. Rev. Lett. **66**, 2332 (1991).
[60] E. Brener, H. Levine, and Y. Tu, Phys. Rev. Lett. **66**, 1978 (1991).
[61] H. Levine and Y. Tu, Phys. Rev. A **45**, 1053 (1992).
[62] R. C. Ball and R. M. Brady, J. Phys. A **18**, L809 (1985).
[63] R. C. Ball, R. M. Brady, G. Rossi, and B. R. Thompson, Phys. Rev. Lett. **55**, 1406 (1985).
[64] M. Kolb, J. Phys. Lett. **46**, L631 (1985); Europhys. Lett. **4**, 85 (1987).
[65] P. Meakin and T. Vicsek, Phys. Rev. A **32**, 685 (1985).
[66] P. Meakin, Phys. Rev. A **33**, 1984 (1986); **33**, 3371 (1986); **36**, 332 (1987).
[67] M. Matsushita and H. Kondo, J. Phys. Soc. Jpn. **55**, 2483 (1986).
[68] J. Nittman and H. E. Stanley, Nature **321**, 663 (1986).
[69] J. Kertész and T. Vicsek, J. Phys. A **19**, L257 (1986).
[70] F. Family, D. E. Platt, and T. Vicsek, J. Phys. A **20**, L1177 (1987).
[71] P. Meakin, R. C. Ball, P. Ramanlal, and L. M. Sander, Phys. Rev. A **35**, 5233 (1987).
[72] S. Tolman and P. Meakin, Phys. Rev. A **40**, 428 (1989).
[73] M. Tabard, Ph.D. thesis, University of Bordeaux, 1993.
[74] A. Arneodo, F. Argoul, E. Bacry, J. F. Muzy and M. Tabard, Phys. Rev. Lett. **68**, 3456 (1992); in *Growth Patterns in Physical Sciences and Biology* (Ref. [17]), p. 191.
[75] A. Arneodo, F. Argoul, J. F. Muzy, and M. Tabard, Phys. Lett. A **171**, 31 (1992); Physica A **188**, 217 (1992).
[76] B. Derrida, V. Hakim, and J. Vannimenus, Phys. Rev. A **43**, 888 (1991).
[77] P. Meakin, Phys. Rev. A **27**, 604 (1983); **27**, 1495 (1983).
[78] P. Meakin, J. Phys. A **18**, L661 (1985).
[79] P. Meakin, Phys. Rev. A **27**, 2616 (1983); Phys. Rev. B **30**, 4207 (1984).
[80] Z. Rácz and T. Vicsek, Phys. Rev. Lett. **51**, 2382 (1983).
[81] P. Meakin, J. Kertész, and T. Vicsek, J. Phys. A **21**, 1271 (1988).
[82] L. Pietronero, A. Erzan, and C. Evertsz, Phys. Rev. Lett. **61**, 861 (1988); Physica A **151**, 207 (1988).
[83] C. Evertsz, J. Phys. A **22**, L1061 (1989); Phys. Rev. A **41**, 1830 (1990).
[84] G. Grasseau, Ph.D. thesis, University of Bordeaux, 1989.
[85] E. Ben Jacob, R. Godbey, N. D. Goldenfeld, J. Koplik, H. Levine, T. Muller, and L. M. Sander, Phys. Rev. Lett. **55**, 1315 (1985).
[86] Y. Couder, O. Cardoso, D. Dupuy, P. Tavernier, and W. Thom, Europhys. Lett. **2**, 437 (1986).
[87] Y. Couder, N. Gerard, and M. Rabaud, Phys. Rev. A **34**, 5175 (1986).
[88] A. Buka, J. Kertész, and T. Vicsek, Nature **323**, 424 (1986).
[89] V. Horvath, T. Vicsek, and J. Kertész, Phys. Rev. A **35**, 2353 (1987).
[90] G. Zocchi, B. E. Shaw, A. Libchaber, and L. P. Kadanoff, Phys. Rev. A **36**, 1894 (1987).
[91] A. R. Kopf-Sill and G. M. Homsy, Phys. Fluids **30**, 2607 (1987).
[92] M. Rabaud, Y. Couder, and N. Gerard, Phys. Rev. A **37**, 935 (1988).
[93] S. K. Sarkar and D. Jasnow, Phys. Rev. A **34**, 5175 (1989).
[94] M. Matsushita and H. Yamada, J. Cryst. Growth **99**, 161 (1990).
[95] H. Thomé, R. Combescot, and Y. Couder, Phys. Rev. A **41**, 5739 (1990).
[96] D. C. Hong and J. S. Langer, Phys. Rev. A **36**, 2325 (1987).
[97] R. Combescot and T. Dombre, Phys. Rev. A **39**, 3525 (1989).
[98] This crossover is similar to that investigated for crystals grown in a narrow channel; see, e.g., D. Kessler, J. Koplik, and H. Levine, Phys. Rev. A **34**, 4980 (1986).
[99] M. Kolb, in *Growth Patterns in Physical Sciences and Biology* (Ref. [17]), p. 221.
[100] H. Levine and Y. Tu, Phys. Rev. E **48**, R4207 (1993).
[101] J. P. Eckmann, P. Meakin, I. Procaccia, and R. Zeitak, Phys. Rev. A **39**, 3185 (1989); Phys. Rev. Lett. **65**, 52 (1990).
[102] B. B. Mandelbrot, J. Stat. Phys. **34**, 895 (1984); in *Fractals' Physical Origin and Properties* (Ref. [13]), p. 3.
[103] M. Muthukumar, Phys. Rev. Lett. **50**, 839 (1983).
[104] M. Tokuyama and K. Kawasaki, Phys. Lett. **100A**, 337 (1984).
[105] K. Honda, H. Toyoki, and M. Matsushita, J. Phys. Soc. Jpn. **55**, 707 (1986).
[106] L. A. Turkevich and H. Scher, Phys. Rev. Lett. **55**, 1026 (1985).
[107] H. G. E. Hentschel, Phys. Rev. Lett. **52**, 212 (1984).
[108] F. Argoul, A. Arneodo, G. Grasseau, and H. L. Swinney, Phys. Rev. Lett. **61**, 2558 (1988); **63**, 1323 (1989).
[109] G. Li, L. M. Sander, and P. Meakin, Phys. Rev. Lett. **63**, 1322 (1989).
[110] F. Argoul, A. Arneodo, J. Elezgaray, G. Grasseau, and R. Murenzi, Phys. Lett. **135A**, 327 (1989); Phys. Rev. A **41**, 5537 (1990).

[111] T. Vicsek, F. Family, and P. Meakin, Europhys. Lett. **12**, 217 (1990).

[112] In fact, these contour plots should be compared with the shape of the stable fingers belonging to the branch $\lambda_{n=0}(\theta_0,B)$ before the merging point with the $\lambda_{n=1}(\theta_0,B)$ branch [46].

[113] A. Arneodo, F. Argoul, E. Bacry, J. F. Muzy, and M. Tabard, Fractals **1**, 629 (1993).

[114] A. Kuhn, F. Argoul, J. F. Muzy, and A. Arneodo, Phys. Rev. Lett. **73**, 2998 (1994).

[115] M. Ben Amar, Europhys. Lett. **16**, 367 (1991).

[116] R. Almgren, W. S. Dai, and V. Hakim, Phys. Rev. Lett. **71**, 3461 (1993).

[117] S. Sandow and S. Trimper, Europhys. Lett. **21**, 799 (1993).